People's Democratic Republic of Algeria
Ministry of Higher Education and Scientific Research

University M'Hamed BOUGARA – Boumerdes

Institute of Electrical and Electronic Engineering

Department of Power and Control

Final Year Project Report Presented in Partial Fulfilment of the Requirements for the Degree of the

"MASTER"

In **Power Engineering**

Option: **Power Engineering**

Title:

Model Predictive Control for FSTP inverter-fed induction motor

Presented by:

- **Ayat Errahmane HAMMADI**

Supervisor:

Mrs. Samira CHALAH

Registration Number:……/2023

Abstract

The rapid growth of electric motor-driven systems has led to an increasing demand for high-performance control strategies that provide efficient and precise operation. Model Predictive Control (MPC) and Direct Torque Control (DTC) have gained significant attention due to their ability to provide fast and accurate control in various industrial applications. The primary objective of this work is to analyze and implement Model Predictive Torque Control (MPTC) for a three-phase induction machine powered by a Four- Switch Three-Phase (FSTP) inverter. The investigation begins with a review of the state-of-the-art on the FSTP inverter and predictive control, highlighting various applications of predictive control. Subsequently, Model Predictive Current Control (MPCC) and MPTC are employed to control an RL-load and an induction machine, respectively, both driven by the FSTP inverter. This work presents a comparative analysis between MPTC and Direct Torque Control (DTC) methods. Simulation of these techniques were then carried out using MATLAB/Simulink software and the obtained results analyzed and discussed to confirm the validity of the proposed techniques.

Acknowledgements

First and foremost, I humbly express my sincere gratitude to Allah Almighty for His abundant blessings, which have endowed me with the ability, knowledge, and strength required to successfully complete my research study.

I would like to express my deepest gratitude and my most sincere appreciations to my advisor **Mrs. Samira CHALAH** for her help and invaluable support. Her remarkable understanding and support have played a pivotal role in creating an environment where I felt comfortable completing this work.

Besides my advisor, I would like to thank **Dr. Abdelkarim AMMAR** for the immense patience and unwavering support and encouragement he has consistently provided me with.

I extend my heartfelt thanks to the esteemed members of the jury who graciously accepted the honor of participating in my committee. I greatly appreciate their time, effort, and commitment in carefully reviewing my work and providing constructive feedback.

I would like to thank each and every individual who has played a part in supporting me throughout my academic journey, right from the very beginning. From the early stages of my studies to the present moment, there have been numerous individuals who have offered their guidance, encouragement, and assistance, and I am truly thankful for their contributions.

Dedication

I dedicate this project to

First and foremost, my loving parents. You have been my unwavering support, my source of strength, and my guiding light since I was a child. I owe everything I have become today and everything I will be in the future to you. I will continuously strive to make you proud as I relentlessly pursue my dreams.

I also want to express my gratitude to my lovely sisters, **Ouidad** and **Nibel**, and my dear brother, **Nidhal**. Your constant presence and support have never faltered, and I am grateful for the bond we share.

To all my family members, I extend my heartfelt appreciation for your support and encouragement throughout this journey. Your belief in me has been invaluable.

To my dear friends, **Wafa**, **Sarra**, **Rahil**, **Abderrahmane**, **Elhachemi**, and **Khireddine**, I am incredibly grateful for your belief in me. Your constant support and encouragement have meant the world to me.

I would also like to thank **Mr. Yacine RAHMANI** and **Mr. Mustapha BOUANANI**. You have been my rock, providing guidance and lending a listening ear whenever I needed it the most. Your faith in my abilities has propelled me forward during moments of doubt and uncertainty, reminding me of my true potential. I am eternally grateful for your presence and unwavering support.

To all those who have played a role in shaping my journey, whether mentioned here or not, thank you. Your support has been instrumental in my growth and achievements.

Ayat Errahmane

Contents

List of Figures

List of Tables

List of symbols and acronyms

FSTP	**F**our **S**witch **T**hree **P**hase
SSTP	**S**ix **S**witch **T**hree **P**hase
MPC	**M**odel **P**redictive **C**ontrol
MPCC	**M**odel **P**redictive **C**urrent **C**ontrol
MPTC	**M**odel **P**redictive **T**orque **C**ontrol
FOC	**F**ield **O**riented **C**ontrol
SVM	**S**pace **V**ector **M**odulation
PWM	**P**ulse **W**idth **M**odulation
THD	**T**otal **H**armonic **D**istortion
IM	Induction motor
M	Neutral point of the inverter
N	Neutral point of the load
T_s	Sampling period
V_{dc}	DC voltage source
ϕ_s	Stator flux
ϕ_r	Rotor flux
i_s	Stator current
i_r	Rotor current
v_s	Stator voltage
v_r	Rotor voltage
L_m	Magnetizing inductance
L_s	Stator inductance
L_r	Rotor inductance
R_s	Stator resistance
R_r	Rotor resistance
M_s	Mutual inductance between two stator windings
M_r	Mutual inductance between two rotor windings
M_{sr}	Magnitude of the inductance between the stator and the rotor
J	Moment of inertia of the mechanical shaft
T_L	Load torque
k_f	Dry friction coefficient
w	Rotor angular speed
p	Number of pole pairs
T_{em}	damping coefficient
w_n	Natural circular pulse

General Introduction

The use of power converters has become very popular in recent decades for a wide range of applications, including drives, energy conversion, traction, and distributed generation. The control of power converters is a vital aspect of their operation, ensuring efficient and reliable energy conversion. Extensive research and development efforts have been devoted to studying power converter control, leading to the emergence of various control schemes and strategies.

Inverters are used to convert the DC power supply into adjustable frequency and voltage AC power, which is necessary for driving and controlling the speed of induction motors. Inverter-driven induction motors offer several advantages over traditional fixed-speed motors, including improved energy efficiency, enhanced control, and reduced mechanical stress. A well-known example is the four-switch three-phase inverter.

Variable speed drives utilizing induction machines have gained significant industrial applications, particularly in electric traction and medium to high-power systems. These drives offer several advantages and are increasingly being adopted in various industries.

The control of power converters and drives has been extensively studied, leading to the development of various control schemes. Hysteresis control and linear control with pulse-width modulation (PWM) are indeed well-established and widely used control techniques. However, advancements in microprocessor technology have enabled the implementation of more sophisticated control schemes, offering improved performance and advanced features. Some of these new control schemes for power converters include fuzzy logic, sliding mode control, and predictive control.

The primary goal of this work is to implement predictive control for the four-switch three-phase (FSTP) inverter connected to an induction machine (IM).

The report is structured into four chapters and can be summarized as follows:

Chapter 1 provides an overview of the four-switch three-phase (FSTP) inverter and the Model Predictive Control (MPC).

Chapter 2 focuses on the modeling of the induction motor and the FSTP inverter. The chapter aims to provide a detailed understanding of the dynamic behavior and characteristics of both the induction motor and the FSTP inverter.

Chapter 3 is dedicated to the analysis and simulation of a Modle Predictive Current Control applied to a FSTP inverter. The inverter feeds power to an RL load and the performance of both the input and output is evaluated.

Chapter 4 delves into the development of a Model Predictive Torque Control (MPTC) approach for an induction machine driven by the FSTP. This chapter commences by introducing MPTC and elucidating its operational principles. The primary goal is to attain accurate control over the torque generated by the induction machine through the utilization of predictive control techniques. Additionally, a comparative analysis is provided, contrasting the merits of MPTC and DTC.

The report concludes with a general summary of the work conducted, highlighting the main results obtained. Additionally, it presents some perspectives for future research and development in the field.

Chapter 1

The FSTP Inverter and The Model Predictive Control: A state of art

1.1 Introduction

The four-switch three-phase (FSTP) inverter and Model Predictive Control (MPC) are key components in the field of power electronics and control systems. The FSTP inverter is a power electronic device used to convert direct current (DC) into three-phase alternating current (AC) with reduced component count and improved efficiency. MPC, on the other hand, is an advanced control technology that utilizes mathematical models and optimization algorithms to achieve precise and dynamic control of a system.

This chapter is divided into two main parts, one is devoted to the state of the art of the FSTP inverter, and the other part is devoted to the state of the art of the Model Predictive Control (MPC). Where the topology of the converter and some applications of the control strategy have been presented.

1.2 State of the art of the FSTP inverter

1.2.1 FSTP inverter topology

In a four-switch three-phase (FSTP) inverter, two of the output load phases are maintained from the two inverter legs, while the third load phase is fed from the DC-link at the middle point of a split-capacitor bank as shown in Figure 1.1 [1]. Recently, the FSTP inverter has attracted the most interest regarding its performance, control, and applications [2]-[3].

1.2.2 The features of the FSTP

Compared to the traditional SSTP inverter, the FSTP inverter has important features such as lower cost and higher efficiency and reduced numbers of measurements, gate drives, and real-time calculations [4]. In addition, the FSTP inverter reduces the maximum common mode voltage by 33% in comparison with the SSTP inverter [4]-[5]. Because of the reduced interaction between switches in the FSTP inverter, switch reliability is increased [2]-[8]-[7].

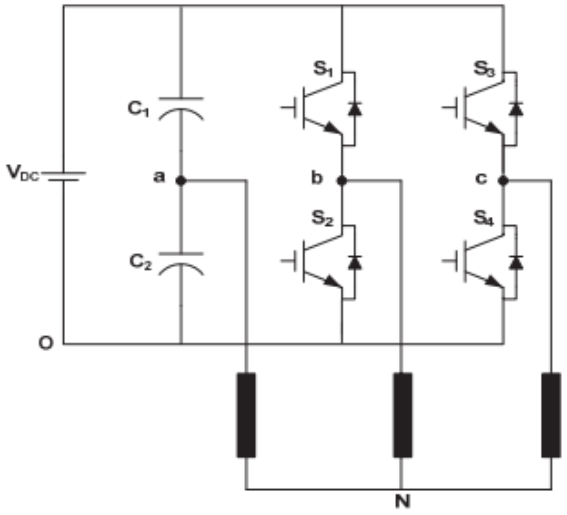

FIGURE 1.1: Conventional FSTP voltage source inverter

1.2.3 The disadvantages of the FSTP inverter

The main disadvantage of the FSTP is that the maximum output voltage across the load is limited to 28.28% of the input dc voltage [8]. Another disadvantage is that the third phase of the output load is fed from the dc side, which may generate dc current components in the output three-phase currents. These dc current components are hazardous and control efforts should suppress them. In addition, the fluctuation of the dc-link capacitor voltage at the fundamental frequency results in fluctuations of the output voltages and currents of the FSTP inverter [9]. The problem of the dc-link voltage oscillation necessitates modified pulse-width modulated(PWM) signals to control and create the desired output voltage during the switching period [10]. Practically, the dc-link split capacitors will not have equal capacitance, so overmodulation of the switch PWM process is needed to maintain a constant dc-link midpoint voltage [9].

1.3 Model Predictive Control

1.3.1 Development of MPC (History)

Model predictive control (MPC) has been extensively studied in the field of control engineering and has garnered significant attention from both industrial and academic researchers [11]. Although "Model Predictive Control" does not refer to a specific control strategy, it encompasses a wide range of control methods that utilize a process model to minimize an objective function and generate the control signal [12]. Predictive control has found successful applications in various domains, including industrial processes, robot manipulators [13], clinical anesthesia, power converters, and drives [12]. The advancement of high-processing microprocessors has overcome the computational burden associated with MPC, enabling its widespread adoption [14].

In a review conducted by the author in [15], three decades of Model Predictive Control (MPC) development were examined. The research revealed that MPC was initially implemented in industries such as oil and petrochemicals as a computer-based supervisory control system, dating back to the 1950s. Despite its promising nature, MPC faced limited adoption in other industrial processes due to the high computational requirements until the mid-1970s.

In the second decade of the MPC development, during the late 1980s, researchers founded a theoretical approach for the MPC: the discrete-time state-space representation model:

$$\begin{cases} x[i+1] = Ax[i] + Bu[i] \\ y[i+1] = Cx[i] + Du[i] \end{cases} \tag{1.1}$$

During this decade, researchers showed interest in studying the stability of the MPC for the first time. This can be proven by considering the cost function of the MPC as a Lyapunov function [15].

1.3.2 Working Principal of MPC

Power converters have seen recent applications of predictive control, which encompasses a broad range of controllers. Classification of different predictive control methods is shown in Figure 1.2.

Hysteresis-based predictive control aims to keep the controlled variable within specific boundaries by anticipating and adapting to system changes. Trajectory-based control guides variables along a predetermined path.

Deadbeat control aims for instant and precise correction, eliminating errors in the next sampling instance. Model predictive control (MPC) uses a cost function and considers future time steps to optimize decisions, minimizing overall cost while balancing performance and stability [16].

These controller groups differ in their need for a modulator to generate voltage. Deadbeat control and continuous control MPC relies on a modulator, resulting in a fixed switching frequency. On the other hand, the other controllers can produce switching signals directly, eliminating the requirement for a modulator and allowing for variable switching frequencies [12].

Model predictive control (MPC) offers several benefits due to its ability to directly incorporate nonlinearities into the system model. Unlike other control schemes, MPC eliminates the need for linearization at a particular operating point, resulting in improved system performance across different conditions. Moreover, MPC provides the flexibility to impose variable restrictions on specific parameters, which is difficult to achieve with control schemes such as deadbeat control. This capability enhances the effectiveness of the control approach and enables better customization and optimization of the system [17].

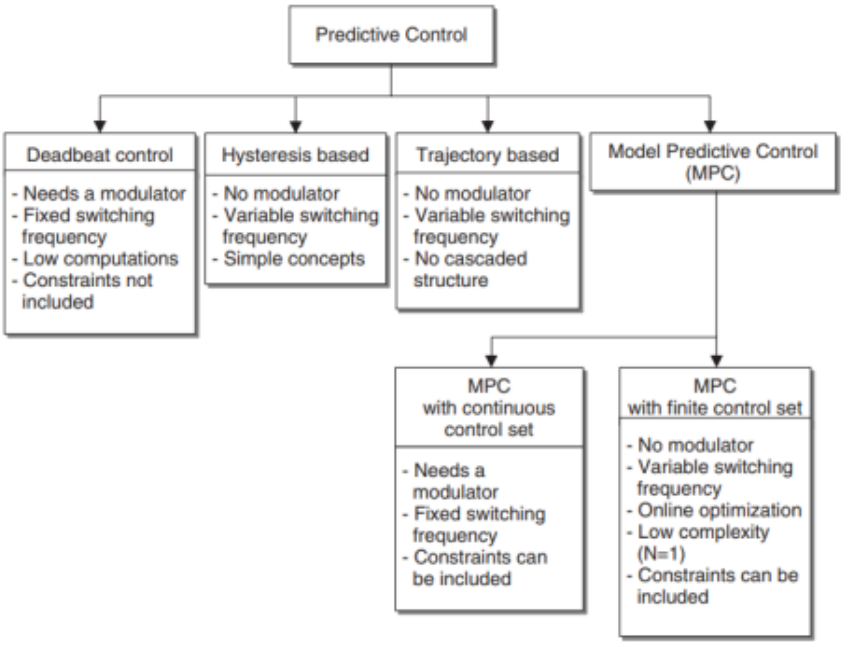

FIGURE 1.2: Classification of predictive control methods used in power electronic

1.3.3 MPC Strategy

The methodology of all the controllers belonging to the MPC family is characterized by the following strategy, represented in Figure 1.3.

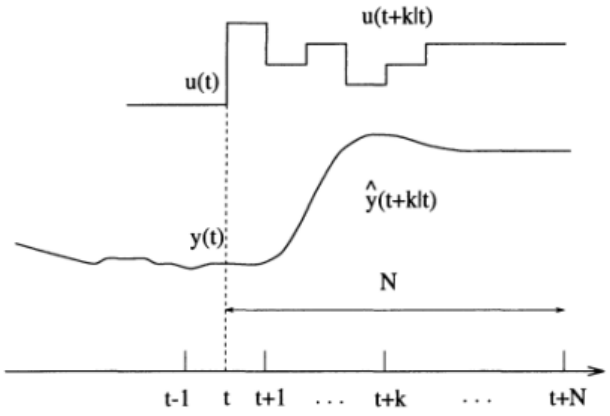

FIGURE 1.3: Working principle of MPC

Model predictive control (MPC) determines the control action by minimizing a cost function that captures the desired behavior of the system. This cost function compares the predicted system output with a reference. The predictions are computed based on the system model. At each sampling time, the MPC controller calculates a sequence of control actions that minimize the cost function. However, only the first

action from this sequence is applied to the system. This repeated algorithm creates a feedback loop, increasing robustness to system uncertainties [18].

1.3.4 MPC's Elements

Figure 1.4 illustrates the essential components comprising the MPC:

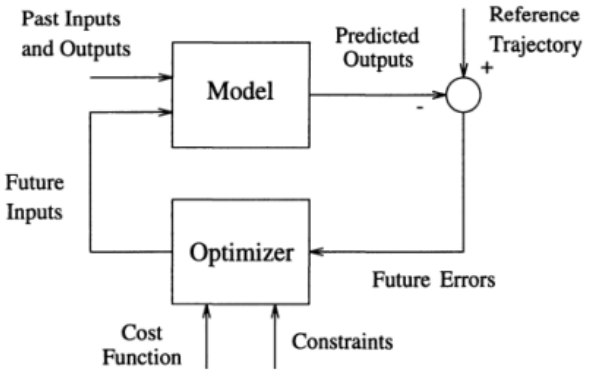

FIGURE 1.4: Basic structure of MPC

1.3.5 Prediction Model

The model is the corner-stone of MPC [11]; a complete design should include the necessary mechanisms for obtaining the best possible model, which should be complete enough to fully capture the process dynamics and should also be capable of allowing the predictions to be calculated and at the same time, to be intuitive and to permit theoretic analysis.

Practically every possible form of modeling a process appears in a given MPC formulation, the following being the most commonly used:

1. Transfer function
2. State Space

Non-linear models can also be used to represent the process but the problem of their use springs from the fact that they cause the optimization problem to be more complicated. Neural nets [18]as well as fuzzy logic [19] are other forms of representation used in some applications.

1.3.6 Objective Function

The various MPC algorithms propose different cost functions for obtaining the control law. The cost function definition is one of the most important stages in the design of an MPC since it allows not only to select the control objectives of the application but also to include any required constraints [20].

This function considers the references, future states (or predicted states), and future actions. In the case of a multivariable system, the cost function may be written as:

$$J = \sum_{i}^{n} \lambda_i |x_i^* - x_i^p| \tag{1.2}$$

where:
n: is the number of controlled variables
x_i: is the controlled variable(It is not written in the function but , it is just to mention the controlled variable)
x_i^*: is the reference value of the controlled variable
x_i^p: is the predicted value of the controlled variable
λ_i: is the weighting factor

The weighting factor allows for adjusting the importance of each controlled variable according to its priority in the scope statement.

The selected actuation is the one that minimizes the cost function, it is stored so that it can be applied to the converter in the upcoming sampling period [21].

1.3.7 Obtaining the control law

In order to obtain values u (t + k | t) which is mentioned in Figure 1.3 it is necessary to minimize functional J. To do this the values of the predicted outputs y(t + k | t) are calculated in function of past values of inputs and outputs and of future control signals, making use of the model chosen and substituted in the cost function, obtaining an expression whose minimization leads [22].

When dealing with a nonlinear system, linear Model Predictive Control (MPC) can still be utilized, provided that the system can be adequately linearized. Linear MPC leverages the benefits of convex optimization, which enables efficient and tractable solutions to the control problem. However, there are cases where the system cannot be effectively approximated by linearization, necessitating the use of nonlinear MPC.

1.3.8 Applications of MPC

Numerous literature reports highlight the increasing prevalence of electronic system applications. Noteworthy examples include predictive current and torque control of power converters [23], [24], motor drives [25], [26], generators utilized in renewable energy applications [27], [28], and energy storage applications [29], [30]. The advancements in microprocessor technology and the advent of computational burden management techniques [25] have played a pivotal role in enabling these applications to flourish.

Model Predictive Control (MPC) has been widely applied to grid-connected power converters for various purposes, including the integration of renewable energy sources

and enhancing the stability and performance of power systems, for instance: flexible AC transmission systems (FACTS), static synchronous compensators (STATCOMS), active power filters (APFs), unified power flow controller (UPFC) or a converter to control the torque and/or speed of a wind turbine for grid integration of renewable energies [31].

In motor drive applications of Model Predictive Control (MPC), it is common to measure the current and mechanical speed of the motor. However, other important variables such as torque, stator, or rotor flux are typically estimated using either an estimator [32] or the mathematical model of the machine. This approach allows for accurate control even in cases where direct measurement of these variables may not be available or practical.

Another application of the MPC can be found in energy storage systems (ESS) [30], including Grid Frequency Regulation, Peak Shaving and Load Management, Renewable Energy Integration, Microgrid Control, Voltage, and Power Quality Control, Islanding, and Black Start Capability.

1.3.9 The major problem of the MPC

Despite being a well-established technique, Model Predictive Control (MPC) still faces some challenges and limitations.

MPC often struggles with handling uncertainties in the system, such as model mismatches, disturbances, and measurement errors. Improving prediction accuracy and developing techniques to account for and mitigate uncertainties are ongoing research areas in MPC.

The selection and design of the cost function in MPC can significantly affect the control performance [33]. Finding appropriate cost functions and determining the weight coefficients that balance different control objectives remains a challenge, as it requires a deep understanding of the system and its requirements.

MPC relies on solving optimization problems online to determine the optimal control actions [34]. This requirement for real-time optimization can be computationally demanding, especially for complex systems with fast dynamics. Developing efficient optimization algorithms or approximation techniques to reduce the computational burden is an active area of research.

Computation efficiency is a major challenge in MPC [35]. The need for real-time calculations and the complexity of the optimization problem can result in high computational demands. Researchers are continuously exploring ways to improve the computational efficiency of MPC algorithms, such as algorithmic optimizations, parallel processing, and hardware acceleration.

1.4 Conclusion

In this chapter, a state-of-the-art of the major elements of our work is presented. In the first section, we discussed the four-switch three-phase inverter, including its topology, features, and primary challenges. The second section provides a brief description of Model Predictive Control (MPC), including its historical development, working principle, and examples of its applications.

Research on four-switch three-phase inverters has been a subject of interest in the field of power electronics and renewable energy systems, where various topologies and control strategies have been investigated for four-switch three-phase inverters.

Originally developed for chemical processes, MPC has expanded its domain and found successful applications in various fields, including renewable energy systems, power converters, and motor drives.

Chapter 2

Induction Motor and Electrical Drives

2.1 Introduction

Induction motors are widely recognized and extensively used electric motors in a multitude of applications, both in industrial and domestic settings. These motors have gained popularity due to their robust construction, compact size, high reliability, and cost-effectiveness, making them a preferred choice for many motor drive applications.

This chapter provides a comprehensive overview of the basics of induction motors and electrical drives. We explore two types of inverter drives for induction motors: the six-switch three-phase inverter (SSTPI) and the four-switch three-phase (FSTP) inverter. These inverter drives play a crucial role in controlling the speed, torque, and overall performance of induction motors in various applications.

2.2 Inducion Motor Basics

The concept of electromagnetic induction forms the foundation of induction motor technology. The ability to convert electrical energy into mechanical energy through the interaction of magnetic fields has revolutionized the way we harness power. Induction motors have a rich history, dating back to the late 19th century when Nikola Tesla and others pioneered their development.

The design of an induction motor is relatively simple and consists of two main parts, a stationary stator, and a rotating rotor. There are two main classes of induction motors differing in the way their rotors are wound: the wound induction motor and the squirrel cage induction motor.

The motor discussed in this thesis is a three-phase squirrel cage induction motor. The rotor of a squirrel cage induction motor consists of aluminum bars that are short-circuited by connecting them to two end rings so that the rotor generates the induction current and magnetic field by itself. This makes the AC induction motor a robust, rugged, and inexpensive candidate for motor drive systems.

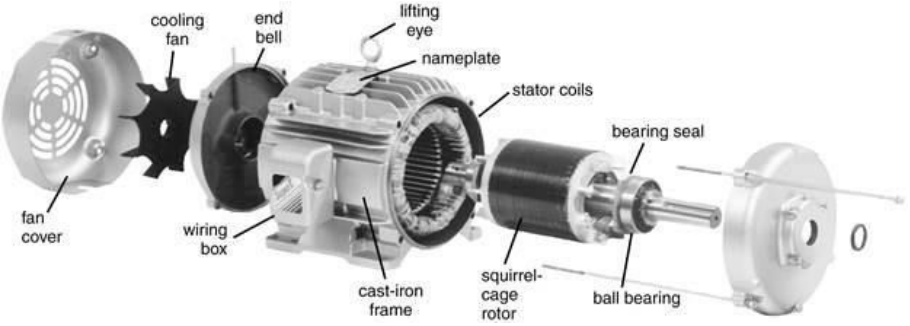

FIGURE 2.1: Induction Motor General Structure

In an induction motor, the alternating currents feed from three-phase terminals and flow through the stator windings, producing a rotating stator flux in the motor. The rotating speed of this magnetic field is defined as synchronous speed, and related to the number of poles of the induction motor and the frequency of the power source.

The rotating magnetic field from the stator will induce a voltage in the rotor bars, since the rotor bars are short-circuited, a large circulating current will be generated in the rotor bars. This induced rotor current will then interact with the rotating magnetic field. Because of Lorentz's law, a tangential electromagnetic force will be generated on the rotor bars, and the sum of forces on each rotor bar produces a torque that eventually drives the rotor in the direction of the rotating field.

When the rotating magnetic field is first generated, the rotor is still in its rest condition. However, the rotor will accelerate rapidly in order to keep up with the rotating stator flux. As the rotor speed increases, the rotor bars are not cut as much by the rotating field, so the voltage in the rotor bars decreases. If the rotor speed equals the flux speed, the rotor bars will no longer be cut by the field and the rotor will start to slow down. This is why induction motors are also called asynchronous motors because the rotor speed will never equal the synchronous speed. The difference between the stator and rotor speed is defined as the slip speed:

$$n_{slip} = n_{sync} - n_m \tag{2.1}$$

$$n_{sync} = \frac{120 f_e}{P} \quad rpm \tag{2.2}$$

where:
n_{slip} is the slip speed
n_{sync} is the speed of the rotating magnetic field
n_m is the mechanical shaft speed of the motor
Also, a slip ratio can be defined as:

$$s = \frac{n_{sync} - n_m}{n_{sync}} \tag{2.3}$$

2.3 Space Vectors

Utilizing space vectors in the modeling of induction motors enables the efficient definition of complex state variables. This approach facilitates the analysis and description of various variables such as three-phase voltages, currents, and fluxes associated with induction motors. Consequently, a comprehensive understanding of these variables can be achieved with ease and convenience.

The three-phase axes are defined by the vectors: e^{j0}, e^{j120}, e^{j240}. The stator windings and stator current space vector in the complex plane are shown below. The space

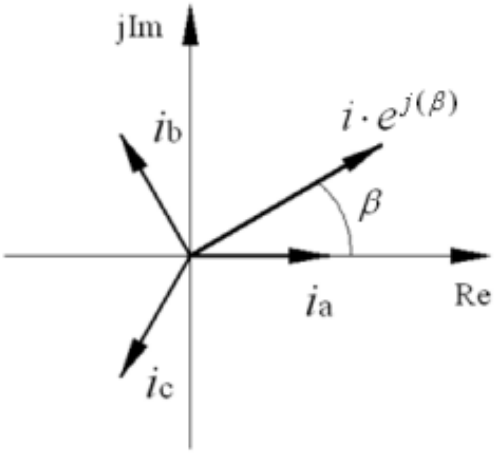

FIGURE 2.2: Current Space Vectors

vector of the stator current $i_s$can be described by:

$$i_s = i_{as}.e^{j0} + i_{bs}.e^{j120} + i_{cs}.e^{j240} \tag{2.4}$$

where the subscript s refers to the stator of the induction motor, a, b, and c are the three phase axes.

Furthermore, the rotor current can be described by:

$$i_r = i_{ar}.e^{j0} + i_{br}.e^{j120} + i_{cr}.e^{j240} \tag{2.5}$$

where the subscript r refers to the rotor of the induction motor.

2.4 The Coordinate Transformation of Space Vectors

The modeling, analysis, and control design of induction motors can be significantly simplified by employing coordinate transformations. These transformations facilitate the conversion of three-phase variables into two-phase variables and the conversion of stationary variables into rotational variables. Key transformations utilized in induction motor control include the Clarke transformation and the Park transformation.

2.4.1 Clarke Transformation

The Clarke transformation transfers a three-phase system into a two-phase system. Take the currents, for example:

$$\begin{bmatrix} i_\alpha \\ i_\beta \end{bmatrix} = \begin{bmatrix} i_a \\ i_b \\ i_c \end{bmatrix} \cdot \begin{bmatrix} 2/3 & -1/3 & -1/3 \\ 0 & \sqrt{3} & -\sqrt{3} \end{bmatrix} \tag{2.6}$$

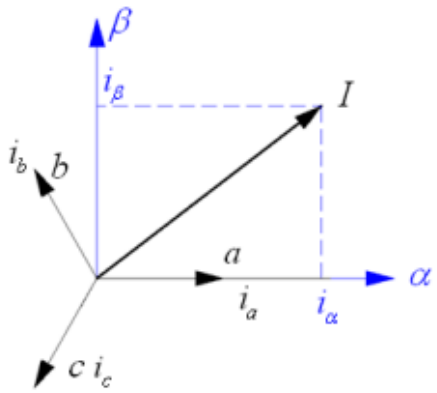

FIGURE 2.3: Clarke transformation of three-phase currents

To make the transformation invertible a third row is added as shown below:

$$\begin{bmatrix} i_\alpha \\ i_\beta \\ i_0 \end{bmatrix} = \begin{bmatrix} 2/3 & -1/3 & -1/3 \\ 0 & \sqrt{3} & -\sqrt{3} \\ 1/3 & 1/3 & 1/3 \end{bmatrix} \cdot \begin{bmatrix} i_a \\ i_b \\ i_c \end{bmatrix} \tag{2.7}$$

The third row represents the zero-sequence component which under balanced conditions is null, i.e.:

$$i_0 = i_a + i_b + i_c \tag{2.8}$$

2.4.2 Park Transformation

From the rotor point of view, all the variables can be observed as constant values. Park's transformation is a revolution in machine analysis, has the unique property of eliminating all time varying inductances from the voltage equations of three-phase ac machines due to the rotor spinning. Hence, the Park transformation transfers a stationary system into a rotational system:

$$\begin{bmatrix} i_d \\ i_q \end{bmatrix} = \begin{bmatrix} i_a \\ i_b \end{bmatrix} \cdot \begin{bmatrix} \cos\theta & \sin\theta \\ -\sin\theta & \cos\theta \end{bmatrix} \tag{2.9}$$

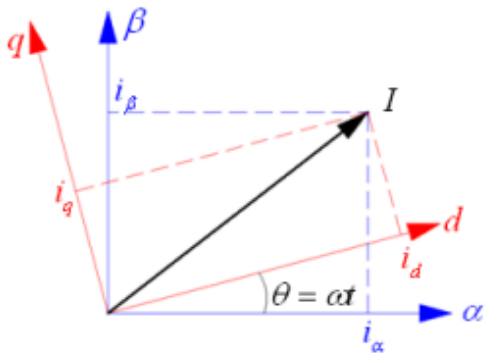

FIGURE 2.4: Park transformation of two-phase currents

2.5 Induction Motor Modelling

Induction motor modeling entails creating mathematical equations and models that accurately depict the electrical and mechanical aspects of the motor. These models are crucial for analyzing and forecasting the motor's performance across various operating conditions.

In the modeling process of an induction motor, electromagnetic laws and motion equations are applied to the windings and rotor carrying the load. This involves incorporating Maxwell's equations and Faraday's law of electromagnetic induction to describe the electrical behavior of the motor, along with mechanical equations that govern the motion of the rotor. By combining these principles, a comprehensive model of the induction motor can be developed.

2.5.1 Flux Equation

There are three kinds of fluxes: stator flux, rotor flux, and mutual flux. The stator flux and rotor flux vectors can be expressed in terms of stator current i_s and rotor current i_r, given below:

$$\psi_{abcs} = L_s.I_{sabc} + L_{mr}.L_{rabc} \tag{2.10}$$

$$\psi_{abcr} = I_{rabc} + L_{ms}.L_{sabc} \tag{2.11}$$

where

$$\left[\psi_{abcs}\right] = \begin{bmatrix} \psi_{as} \\ \psi_{bs} \\ \psi_{cs} \end{bmatrix} \; and \; \left[\psi_{abcr}\right] = \begin{bmatrix} \psi_{ar} \\ \psi_{br} \\ \psi_{cr} \end{bmatrix}$$

$$\left[I_{abcs}\right] = \begin{bmatrix} I_{as} \\ I_{bs} \\ I_{cs} \end{bmatrix} \; and \; \left[I_{abcr}\right] = \begin{bmatrix} I_{ar} \\ I_{br} \\ I_{cr} \end{bmatrix}$$

$$\left[L_s\right] = \begin{bmatrix} l_s & M_s & M_s \\ M_s & l_s & M_s \\ M_s & M_s & l_s \end{bmatrix} \; and \; \left[L_r\right] = \begin{bmatrix} l_r & M_r & M_r \\ M_r & l_r & M_r \\ M_r & M_r & l_r \end{bmatrix}$$

and

$$\left[L_m\right] = M \begin{bmatrix} \cos(p\theta) & \cos(p\theta + \frac{2\pi}{3}) & \cos(p\theta + \frac{4\pi}{3}) \\ \cos(p\theta + \frac{4\pi}{3}) & \cos(p\theta) & \cos(p\theta + \frac{2\pi}{3}) \\ \cos(p\theta + \frac{4\pi}{3}) & \cos(p\theta + \frac{2\pi}{3}) & \cos(p\theta) \end{bmatrix}$$

L_s and L_r are the stator inductance and the rotor inductance, respectively; L_m is the mutual inductance between the stator and rotor windings. M presents the maximal mutual inductance between the stator phase and the rotor phase. p designates the number of pole pairs and θ denotes the angle between the stator and the rotor.

2.5.2 Voltage Equation

The stator and rotor voltage equations are given by:

$$V_{sabc} = R_s * I_{sabc} + \frac{d}{dt} * \phi_{sabc} \tag{2.12}$$

$$0 = V_{rabc} = R_r * I_{rabc} + \frac{d}{dt} * \phi_{rabc} \tag{2.13}$$

where:

$$\left[V_{abcs}\right] = \begin{bmatrix} V_{as} \\ V_{bs} \\ V_{cs} \end{bmatrix} \; and \; \left[V_{abcr}\right] = \begin{bmatrix} V_{ar} \\ V_{br} \\ V_{cr} \end{bmatrix}$$

$$\left[\phi_{abcs}\right] = \begin{bmatrix} \phi_{as} \\ \phi_{bs} \\ \phi_{cs} \end{bmatrix} \; and \; \left[\phi_{abcr}\right] = \begin{bmatrix} \phi_{ar} \\ \phi_{br} \\ \phi_{cr} \end{bmatrix}$$

and

$$\left[R_s\right] = \begin{bmatrix} R_s & 0 & 0 \\ 0 & R_s & 0 \\ 0 & 0 & R_s \end{bmatrix} \; and \; \left[R_r\right] = \begin{bmatrix} R_r & 0 & 0 \\ 0 & R_r & 0 \\ 0 & 0 & R_r \end{bmatrix}$$

2.5.3 Mechanical Equation

The rotor motion undergoes the following usual second-order differential equation :

$$J\frac{dw_m}{dt} = -Fw_m + T_{em} - T_L - T_d \tag{2.14}$$

where : w_m, T_L, T_{em}, and T_d are, respectively, the rotor speed, the load torque, the electromagnetic motor torque, and the dry torque. J designates the inertia of the rotor-load set and F the viscous friction coefficient. The expression of T_{em} obtained from the energy balance and it's shown bellow:

$$T_{em} = \frac{\delta W_{mag}}{\delta \theta} \tag{2.15}$$

with:

$$W_{mag} = \frac{1}{2}([I_{sabc}]^T * \phi_{sabc} + [I_{rabc}]^T * \phi_{rabc}) \tag{2.16}$$

2.6 Simulation of the model of the machine

To model the induction motor, an open-loop simulation has been done in MATLAB/Simulink environment with and without load torque at start-up. The induction machine is fed by its nominal three-phase voltage source. The machine parameters are given in Table D.1 in Appendix D.

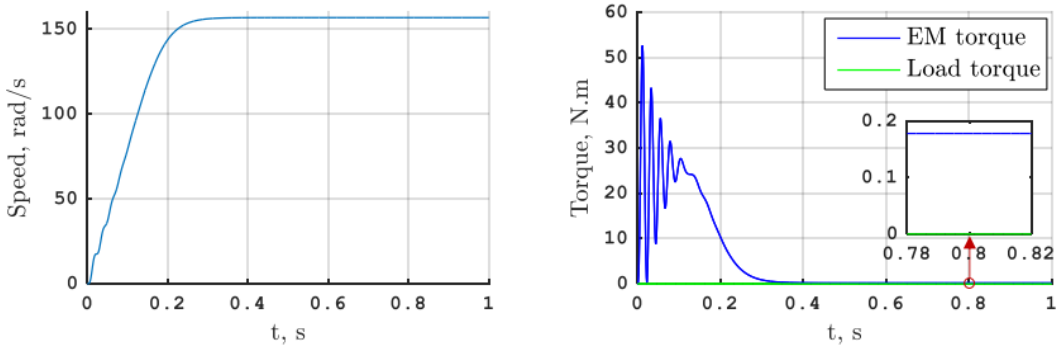

(a) (b)

FIGURE 2.5: Open-loop, no load simulation and results of the induction motor model: (a) mechanical speed, (b) electromagnetic and load torque

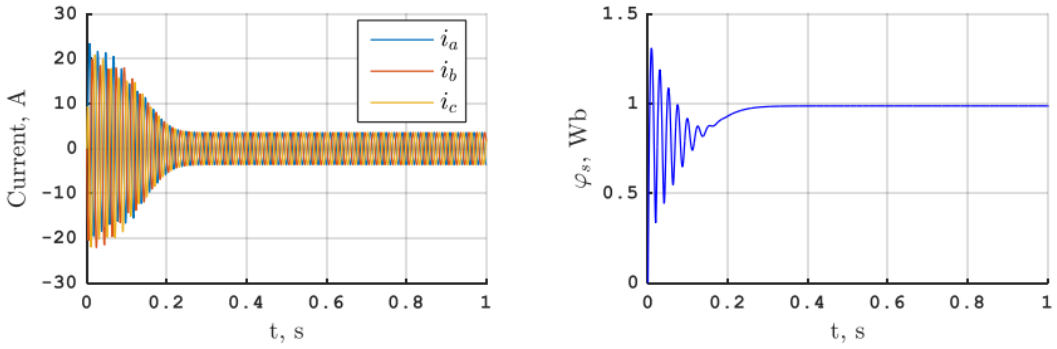

(a) (b)

FIGURE 2.6: Open-loop, no load simulation and results of the induction motor model: (a) stator currents, (b) stator flux magnitude

Figure 2.5 and Figure 2.6 display the results of an open-loop simulation without any load for the induction motor model. In Figure 2.5(a), it is evident that the motor reaches a steady-state speed of 156.8634 rad/s, which closely aligns with its nominal value of 1500 rpm or 157.0792 rad/s. This slight difference can be attributed to the slip, a crucial characteristic of induction machines.

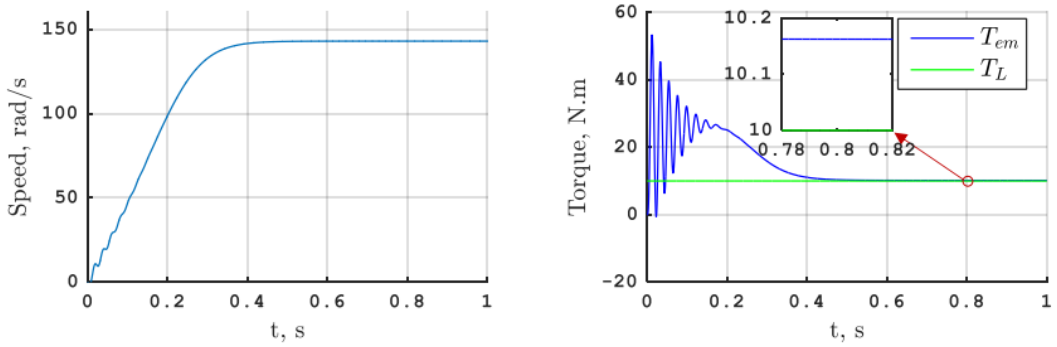

(a) (b)

FIGURE 2.7: Open-loop, with load simulation and results of the induction motor model: (a) mechanical speed, (b) electromagnetic and load torque

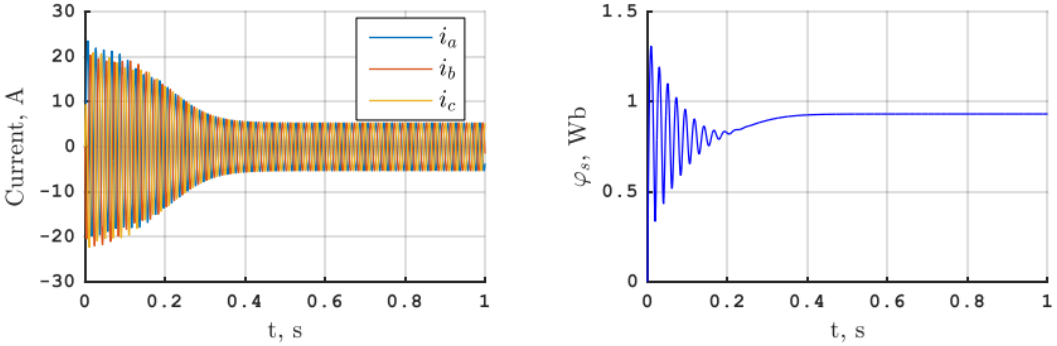

(a) (b)

FIGURE 2.8: Open-loop, with load simulation and results of the induction motor model: (a) stator currents, (b) stator flux magnitude

Figure 2.5(b) demonstrates that even in the absence of load torque, the electromagnetic torque remains nonzero at a steady state due to the presence of the dry friction coefficient k. The difference is the product of the mechanical speed and k.

Moving on to Figure 2.7 and Figure 2.8, which depict an open-loop simulation with a load for the induction motor model. In Figure 2.7(a), it is evident that the mechanical speed does not reach its nominal value and stops at 142.9688 rad/s.

Similar to the previous scenario, Figure 2.7(b) reveals that the electromagnetic torque slightly surpasses the load torque due to the dry friction coefficient k_y. Consequently, the stator current magnitude is higher at steady state compared to the previous case (3.6059 A in Figure 2.6(a) and 5.3368 A in Figure 2.7(a)).

2.7 Variable Frequency Drives

Induction or alternating current (AC) electric motors rotate at a rate determined by the number of poles within the motor and the frequency of the power supply. This is known as the synchronous speed of the motor. The frequency (measured in Hertz) is

directly related to the Revolutions Per Minute (RPM) of a motor. The higher the frequency, the faster the RPM or the higher the engine rotation speed. When motors are supplied directly from the power network, the supply power frequency is constant, (50 Hz/60 Hz).To manage the speed when necessary, additional mechanical systems are used: dampers, valves, gearboxes, brakes, etc. However, these mechanical systems introduce inefficiencies into the overall system.

By using VFDs, the need for additional mechanical systems to control motor speed is eliminated, resulting in increased overall system efficiency. Three main sections rectifier, filter with energy storage, and inverter-VFDs provide precise and smooth control over motor speed, allowing for energy savings, improved process control, and reduced mechanical stress on the motor.

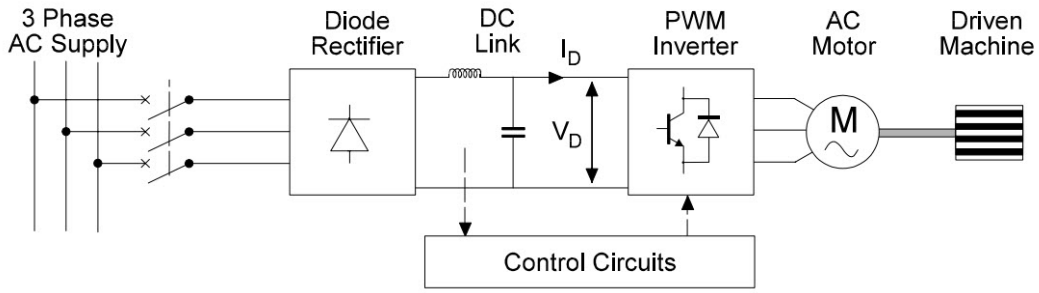

FIGURE 2.9: Variable Frequency Drive Configuration

The rectifier circuit is responsible for converting the incoming AC power supply into DC power. The rectifier can be either a diode rectifier or a more advanced thyristor-based rectifier, such as a 6-pulse or 12-pulse rectifier. The rectified DC voltage is then filtered to smooth out any ripples.

The DC link section serves as an energy storage unit. It consists of a DC bus capacitor that maintains a stable DC voltage level by absorbing and releasing energy. This capacitor helps provide a constant voltage source for the subsequent sections of the VFD.

The inverter section converts the DC voltage from the DC link into a variable-frequency AC voltage. It typically uses insulated gate bipolar transistors (IGBTs) or power MOSFETs to switch the DC voltage at high frequency, producing a pulse-width modulated (PWM) waveform. By controlling the switching pattern and pulse width of the PWM signals, the inverter section generates an adjustable output voltage with a variable frequency.

The control section of a VFD manages and regulates the operation of the drive. It includes a microprocessor or digital signal processor (DSP) that executes control algorithms to achieve the desired motor speed and torque control. This section receives input signals, such as speed references and feedback from sensors, and processes them to generate appropriate control signals for the power conversion and inverter sections.

2.8 Control Methods of Induction Motor

In the past few decades, for general objectives, such as improved performance, high energy efficiency, and increased safety levels, researchers have been investigating IM control from different directions. One of the approaches is from a hardware aspect, such as improving the semiconductor switches; multi-level inverters, and additional phases of motor winding. Another approach is the control theory development, due to the digital control platforms that are well developed and extensively applied in power electronics applications. Modern control engineering had significantly developed since the early 20th century, due to the advance in technology.

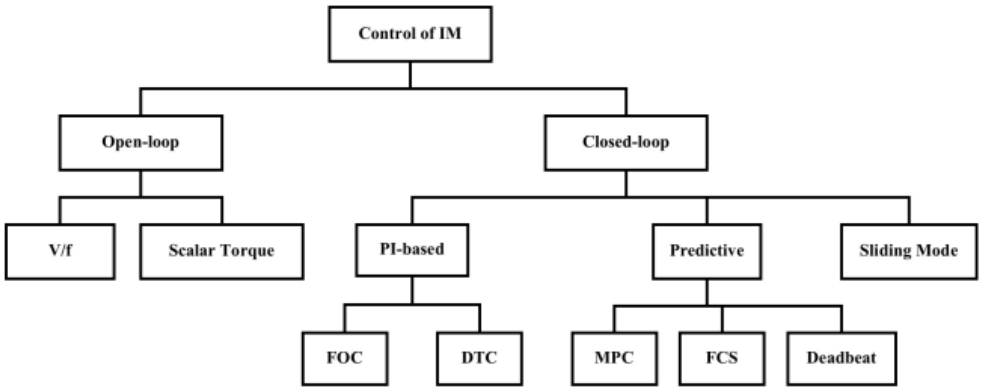

FIGURE 2.10: Control methods of Induction Motor

In the early days, the induction motor speed was adjusted by using the silicon-controlled rectifier back in the 1960s, after that, the variable-frequency v/f control was investigated and even today still commonly used for applications with low-performance requirements. The high-performance control of induction motor drive was not found until the Field Oriented Control (FOC) become the industry standard for AC motor drive, since it transforms the AC motor dynamics close to a DC motor.

Figure 2.10 illustrates the categories of popular control theories for induction motor drives. Among them, FOC and Direct Torque Control (DTC) are more like methodology than theory. To differ from new control algorithms, they were placed under PI-based control.

The idea of FOC was developed based on the electromagnetic torque proportional to the cross-product of stator current and rotor flux, which decoupled the control of torque and filed excitation, similar to a DC motor [36]. Alternatively, the DTC employs hysteresis control directly with stator flux and torque references based on a lookup table [37].

FOC and DTC are well-established control strategies with proven performance in motor control applications. MPC, on the other hand, offers advanced control capabilities by considering future predictions and optimizing control actions based on

defined objectives and constraints. MPC can provide superior performance but requires more computational resources and expertise for implementation by considering future predictions and optimizing control actions based on defined objectives and constraints.

2.9 Voltage Source Inverter

Voltage Source Inverters are used to transfer real power from a DC power source to an AC load. Usually, the DC source voltage is nearly constant and the amplitude of the AC output voltage is controlled by adopting a suitable control strategy. Areas, where VSIs are used, include adjustable speed drives for AC motors, Electronic frequency changer circuits, etc. VSIs are also becoming widely adopted for other applications such as grid connection for renewable energy sources, where a variable voltage DC power source supplies power to an AC system with a nearly constant voltage. There are three main types of VSI namely Single-Phase Half Bridge Inverters, single-phase full-bridge inverters, and three-phase voltage source inverters.

2.9.1 Six Switch Voltage Source Inverter

Figure 2.11 shows the power circuit of a three-phase voltage source inverter.

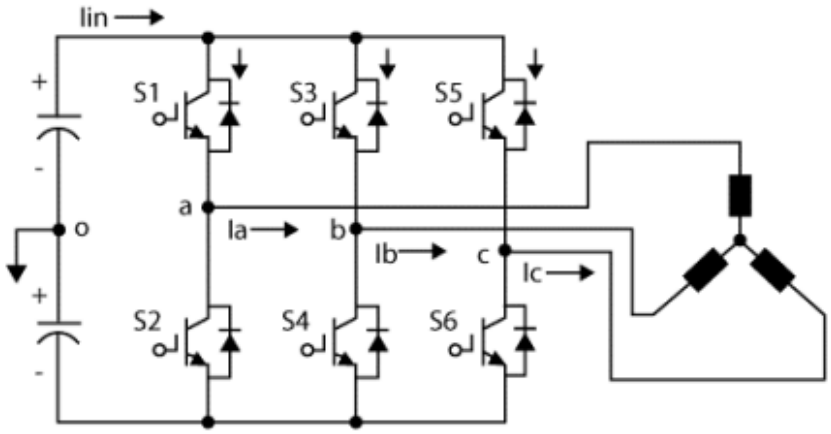

FIGURE 2.11: Six Switch Inverter

The leg voltages are denoted by V_A, V_B, V_C where the relationship between the leg voltage ans switching signals is given by:

$$V_K = (S_K - 0.5) * V_{dc} \qquad K \in (A, B, C) \tag{2.17}$$

Where S_K = 1 when the upper power switch is 'ON' and S_K = 0 when the lower switch is 'ON'.

To avoid shorting the DC rail, the upper and the lower switches are complimentary. The total possible outputs are $(2^3) = 8$(000,001,010,011,100,101,110,111).Thus, there are six active switching states and two zero switching states. The space vectors are shown graphically in complex plan $\alpha\beta$ in Figure 2.9

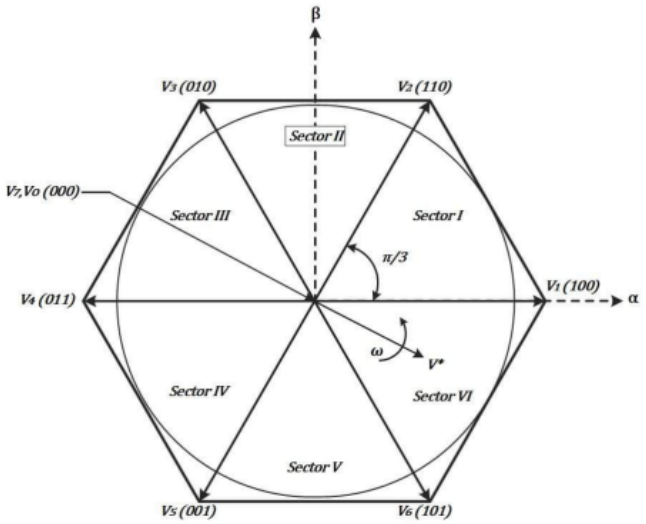

FIGURE 2.12: Different voltage vectors generated by a six-switch inverter

The following expressions present a model of three-phase inverter:

$$\begin{bmatrix} V_{an} \\ V_{bn} \\ V_{cn} \end{bmatrix} = (\frac{V_{dc}}{3}) \begin{bmatrix} 2 & -1 & -1 \\ -1 & 2 & -1 \\ -1 & -1 & 2 \end{bmatrix} \begin{bmatrix} S_a \\ S_b \\ S_c \end{bmatrix} \tag{2.18}$$

TABLE 2.1: Switching states and voltage vectors

S_a	S_b	S_c	Voltage vector $\mathbf{V}$
0	0	0	$\mathbf{V}_0 = 0$
1	0	0	$\mathbf{V}_1 = \frac{2}{3}V_{dc}$
1	1	0	$\mathbf{V}_2 = \frac{1}{3}V_{dc} + j\frac{\sqrt{3}}{3}V_{dc}$
0	1	0	$\mathbf{V}_3 = -\frac{1}{3}V_{dc} + j\frac{\sqrt{3}}{3}V_{dc}$
0	1	1	$\mathbf{V}_4 = -\frac{2}{3}V_{dc}$
0	0	1	$\mathbf{V}_5 = -\frac{1}{3}V_{dc} - j\frac{\sqrt{3}}{3}V_{dc}$
1	0	1	$\mathbf{V}_6 = \frac{1}{3}V_{dc} - j\frac{\sqrt{3}}{3}V_{dc}$
1	1	1	$\mathbf{V}_7 = 0$

In addition, any three-phase system defined by: $V_{an}(t), V_{bn}(t), V_{cn}(t)$ can be represented uniquely by a rotating vector V_s:

$$V_s = \frac{2}{3} * [v_{an} + V_{bn}.e^{j\frac{2\pi}{3}} + V_{cn}.e^{j\frac{4\pi}{3}}] \tag{2.19}$$

2.9.2 Four Switch Voltage Source Inverter

The circuit of the FSTP voltage source inverter is shown in Figure 2.13. This circuit is composed of two sides; the first side consists of two IGBT switches Q1, Q2 and two capacitors C1, C2 together constitute a single-phase half-bridge rectifier circuit, the remaining four IGBTs and the capacitor C1, and C2 together form a low-cost four-switch three-phase inverter circuit.

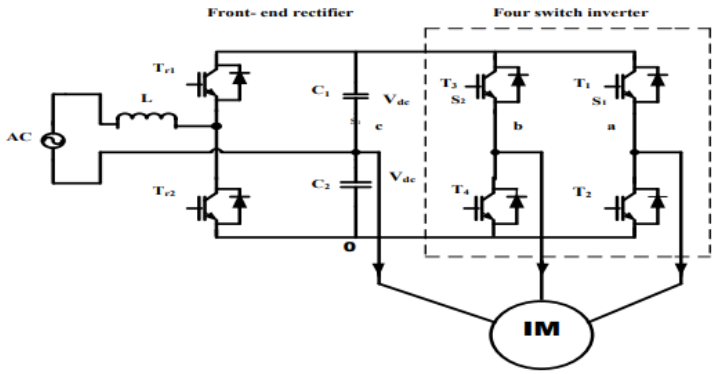

FIGURE 2.13: FSTP Voltage Source Inverter

The rectifier provides the dc link voltage for the inverter and the inverter is followed by a three-phase induction motor. Phase “a” and phase “b” of the IM are connected through two limbs of the inverter, while phase “c” is connected to the midpoint of the capacitors bank, The maximum dc link voltage across each capacitor maintains equal to V_{dc}.

According to the scheme in Figure 2.13 the switching status of the inverter is represented by binary variables S1 to S4, which are set to "1" when the switch is closed and "0" when open. In addition, the switches in one inverter branch are controlled complementary (1 on, 1 off), therefore:

$$S1 + S4 = 1$$

$$S2 + S3 = 1$$

The phase to the common point c voltage depends on the turning off signal of the switch as in:

$$\begin{cases} V_{ao} = (2S_1 - 1)\dfrac{V_{dc}}{2} \\ V_{bo} = (2S_2 - 1)\dfrac{V_{dc}}{2} \\ V_{co} = 0 \end{cases} \tag{2.20}$$

Under balanced conditions, the following equations are obtained:

$$\begin{cases} V_{an} + V_{bn} + V_{cn} = 0 \\ V_{ao} + V_{bo} + V_{co} - 3V_{no} = 0 \\ V_{no} = \dfrac{1}{3}(V_{ao} + V_{bo} + V_{co}) \end{cases} \tag{2.21}$$

From the equations and the phase-to-neutral voltages can be derived as follow:

$$\begin{cases} V_{an} = \dfrac{V_{dc}}{3}(4S_1 - 2S_4 - 1) \\ V_{bn} = \dfrac{V_{dc}}{3}(4S_2 - 2S_3 - 1) \\ V_{cn} = -\dfrac{V_{dc}}{3}(4S_1 + S_2 - 1) \end{cases} \tag{2.22}$$

Since there are 2 switches $S_1 and S_2$ that control the output voltage, then there exists $2^2 = 4$ possible positions of the voltage space vector from the combination of the switching states, in which all the vectors are active (V_1, V_2, V_3, V_4) and there is no zero vector [38]. The four switching states are shown as space vectors in Figure 2.14.

The alpha-beta plane is divided into 4 sectors 90 degrees each and given as:

Sector 1	Sector 2	Sector 3	Sector 4
$-30^0 + 60^0$	$60^0 + 150^0$	$150^0\ 240^0$	$240^0\ -30^0$

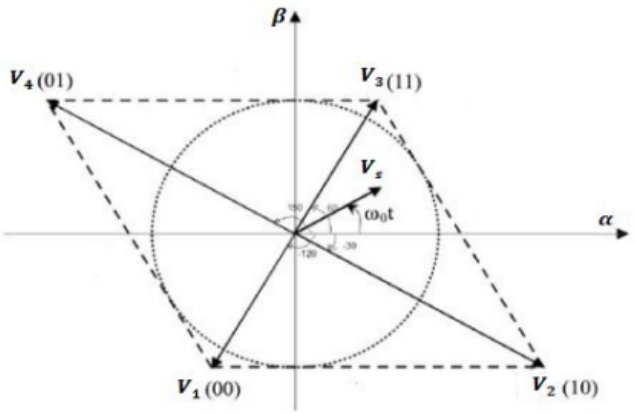

FIGURE 2.14: Voltage space vector of FSTPI in the $\alpha\beta$ plan

TABLE 2.2: FSTP inverter modes of operation

Switching Function		Switch on		Output Voltage Vector		
S_a	S_b			V_a	V_b	V_c
0	0	Q_4	Q_3	$-V_{dc}/3$	$-V_{dc}/3$	$2V_{dc}/3$
0	1	Q_4	Q_2	$-V_{dc}$	V_{dc}	0
1	0	Q_1	Q_3	V_{dc}	$-V_{dc}$	0
1	1	Q_1	Q_2	$V_{dc}/3$	$V_{dc}/3$	$-2V_{dc}/3$

2.10 Linear Control with Pulse Width Modulation or Space Vector Modulation

Considering a modulator stage for the generation of control signals for the power switches of the converter allows one to linearize the nonlinear converter. In this way, any linear controller can be used, the most common choice being the use of proportional-integral (PI) controllers.

2.10.1 Pulse Width Modulation

In a pulse width modulator, the reference voltage is compared to a triangular carrier signal , and the output of the comparator is used to drive the inverter switches. In a three-phase inverter, the reference voltage of each phase is compared to the triangular waveform, generating the switching states for each corresponding inverter leg, as shown in Figure 2.15. Output voltages for phases a and b, v_{an} and v_{bn}, and line-to-line voltage v_{ab} are also shown in this figure.

2.10.2 Linear Control with Space Vector Modulation

A variation of PWM is called space vector modulation (SVM), in which the application times of the voltage vectors of the converter are calculated from the reference vector. It is based on the vectorial representation of the three-phase voltages, defined as:

$$V = \frac{2}{3}(V_{an} + aV_{bn} + a^2V_{cn}) \tag{2.23}$$

where Va_n , Vb_n, and Vc_n are the phase-to-neutral voltages of the inverter and $a = \exp(j\frac{2\pi}{3})$. The output voltages of the inverter depend on the switching state of each phase and the DC link voltage, $V_{xn} = S_xV_{dc}$, with x = a, b, c. Then, taking into account for the combinations of the switching states of each phase, the three-phase inverter generates the voltage vectors.

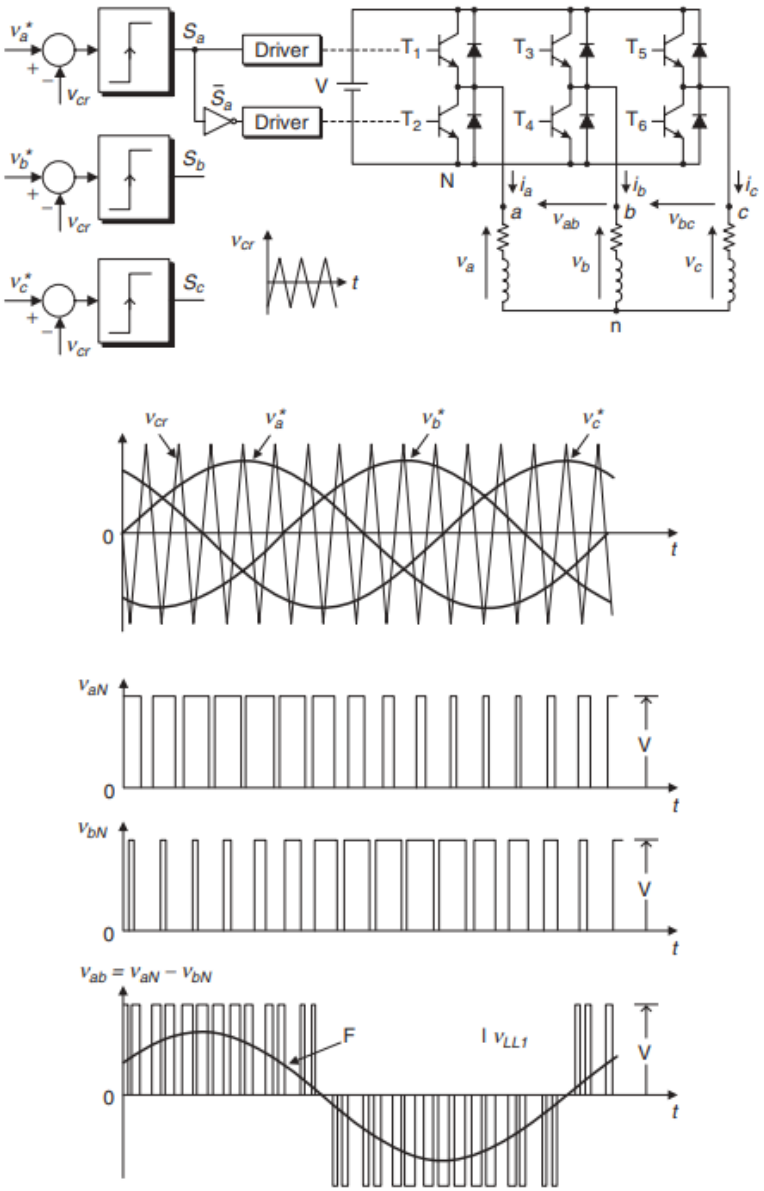

FIGURE 2.15: Pulse width modulator for a three-phase inverter

Considering the voltage vectors generated by the inverter, the $\alpha - \beta$ plane is divided into six sectors, as shown in Figure 2.16. In this way, a given reference voltage vector $V*$, located at a generic sector k, can be synthesized using the adjacent vectors V_k, V_{k+1}, and V_0, applied during t_k, t_{k+1}, and t_0, respectively. This can be summarized with the following equations:

$$V* = \frac{1}{T}(V_k t_k + V_{k+1} t_k + _1 + V_0 t_0) \tag{2.24}$$

$$T = t_k + t_{k+1} + t_0$$

where T is the carrier period and t_k/T , t_{k+1}/T , and t_0/T are the duty cycles of their respective vectors.

Using trigonometric relations the application time for each vector can be calculated, resulting in

$$\begin{cases} t_k = \dfrac{3T|V*|}{2V_{dc}}(\cos(\theta-\theta_k) - \dfrac{\sin(\theta-\theta_k)}{\sqrt{3}}) \\ t_{k+1} = \dfrac{3T|V*|}{2V_{dc}}\dfrac{\sin(\theta-\theta_k)}{\sqrt{3}} \\ t_0 = T - t_k - t_k + 1 \end{cases} \tag{2.25}$$

where θ is the angle of the reference vector$V*$ and θ_k is the angle of vector V_k.

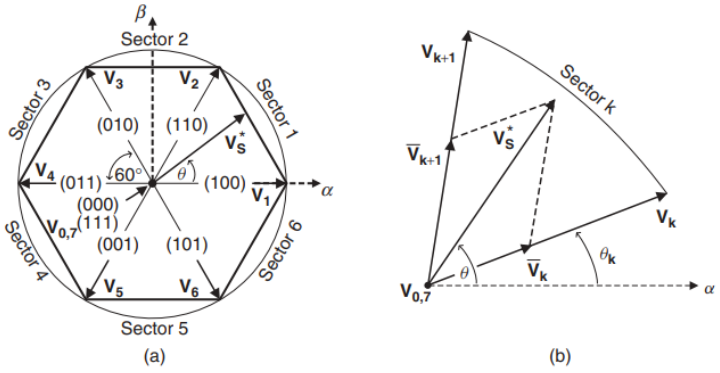

FIGURE 2.16: Principles of space vector modulation (SVM). (a) Voltage vectors and sector definition.(b) Generation of the reference vector in a generic sector

A classical current control scheme using SVM is shown in Figure 2.17. Here, the error between the reference and the measured load current is processed by a PI controller to generate the reference load voltages. With this method, constant switching frequency, fixed by the carrier, is obtained. The performance of this control scheme depends on the design of the controller parameters and on the frequency of the reference current.

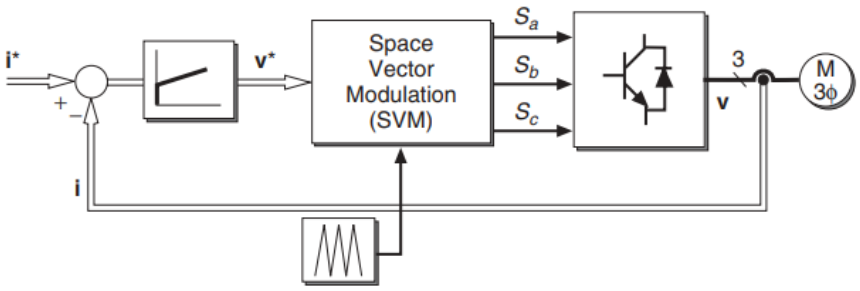

FIGURE 2.17: Classical control scheme using SVM

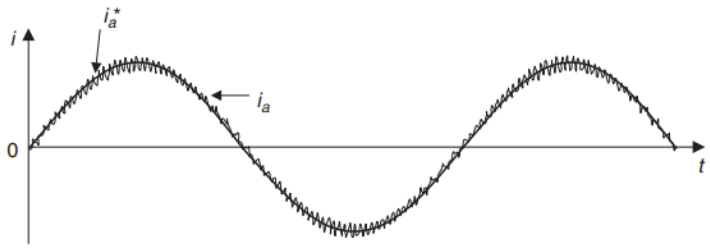

FIGURE 2.18: Load current for a classical control scheme using SVM

2.11 Simulation of SVPWM for the FSTP inverter

To test the feasibility of the suggested structure of the SVPWM for the FSTP inverter, the simulation was run in MATLAB Simulink. The Simulink model of the SVPWM for the FSTP inverter is given in Appendix B.

The reference voltage sine waves have a frequency of 50HZ. The output voltage waveforms for the inverter are produced using a 650 v dc link.

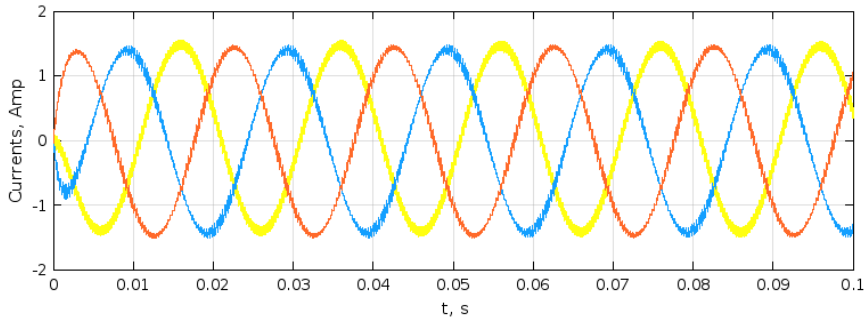

FIGURE 2.19: RL-load current using SVPWM for FSTP inverter

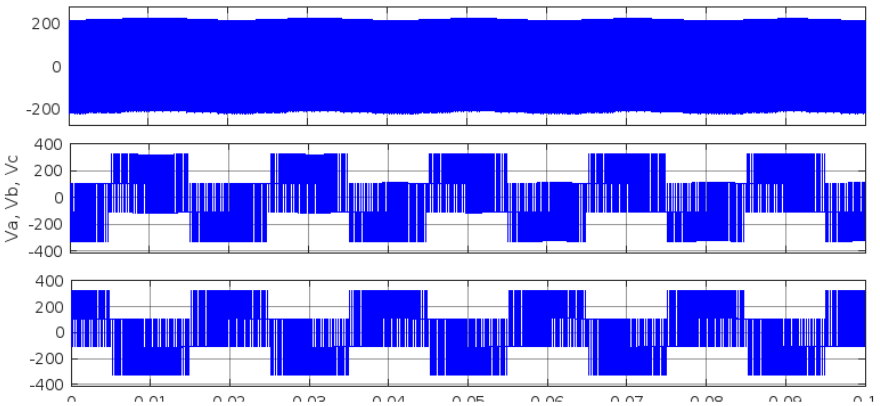

FIGURE 2.20: RL-load phase voltage using SVPWM for FSTP inverter

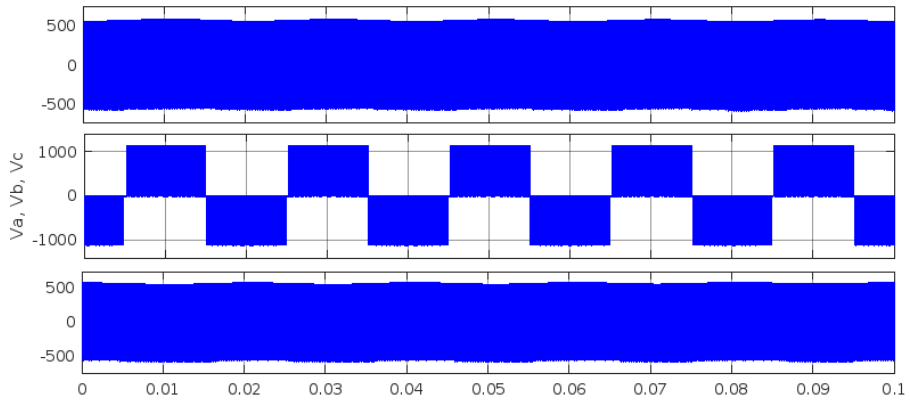

FIGURE 2.21: RL-load line-to-line voltage using SVPWM for FSTP inverter

In order to achieve the line-to-line and phase voltages output waveform, a FSTP inverter with three phase RL load is shown in Figure 2-20, and Figure 2-21 shows the results.

The simulation results include the output current waveform generated by the inverter. We can notice that SVPWM produces a sinusoidal output voltage with low distortion, the waveform closely resembles a pure sinusoid and it meets the desired specifications in terms of magnitude and frequency.

2.12 Conclusion

In conclusion, this chapter provided an overview of induction motors, Variable Frequency Drives (VFDs), and voltage source inverters. Induction motors were discussed, highlighting their construction, working principle, modeling, and control methods. The importance of understanding these fundamentals was emphasized as they form the basis for further discussions on VFDs and voltage source inverters.

VFDs play a vital role in motor control, offering flexibility and efficiency in operating induction motors.

The working principle of VFDs involves adjusting the frequency and voltage supplied to the motor, allowing for precise speed and torque control.

Voltage source inverters, as a common type of power electronic converter used in VFDs, were explored in detail. These inverters convert DC voltage from a power source into a variable frequency and variable voltage AC output. The chapter covered two types of voltage source inverters: the six-switch three-phase (SSTP) inverter and the four-switch three-phase (FSTP) inverter.

Techniques such as Pulse Width Modulation (PWM) were discussed as means to control the switching of power electronic devices within the inverters and generate the desired output waveform.

Chapter 3

Model Predictive Current Control of a FSTP Inverter-Fed RL-Load

3.1 Introduction

Recently, different research works to design new power converters for minimizing losses and costs have been proposed. Four-switch three-phase (FSTP) inverters instead of SSTP inverters have been used in many applications. With technological development, interest has been shown to Model Predictive Current Control (MPCC).

This chapter presents an MPC scheme for a four-switch three-phase inverter fed RL-load. The modeling of the load will be presented, the working principle will be explained and both simulation and experimental results will be shown.

3.2 Model Predictive Current Control

In model predictive current control (MPCC), the goal is to control a system by predicting its future behavior using a model and optimizing the control inputs to achieve desired performance where the variable to be controlled is the current.

The MPC algorithm uses a model of the system to predict the future values of the current based on different possible switching states of the inverter. The predicted output current values are then compared to a reference value or trajectory that represents the desired behavior of the system.

By comparing the predicted output currents with the reference, the MPC algorithm determines the optimal switching state of the inverter that minimizes the deviation from the desired behavior. This optimal switching state is then applied to the inverter, and the process is repeated in a receding horizon manner, where the control inputs are continuously updated based on the most recent measurements and predictions.

3.3 Load Model

The application of Kirchhoff's first law to the RL-load gives:

$$\begin{cases} u_1 = L\dfrac{di_a}{dt} + Ri_a \\ u_2 = L\dfrac{di_b}{dt} + Ri_b \\ u_1 = L\dfrac{di_c}{dt} + Ri_c \end{cases} \tag{3.1}$$

By transforming (3.1) into Laplace domain as transfer functions, to get a model for this RL load for simulation in MATLAB/Simulink environment we get:

$$\begin{cases} \dfrac{i_a}{u_1} = \dfrac{1}{sL+R} \\ \dfrac{i_b}{u_2} = \dfrac{1}{sL+R} \\ \dfrac{i_c}{u_3} = \dfrac{1}{sL+R} \end{cases} \tag{3.2}$$

To achieve a precise control strategy, a forward Euler method discretization of the system (3.2) is used to accurately predict the future values of the output current at the sampling period Ts. So $\frac{di}{dt}$ is replaced by $\frac{i[k+1]i[k]}{T_s}$ and after some arrangements, (3.2) becomes:

$$\begin{cases} i_a[k+1] = (1 - \dfrac{RT_s}{L})i_a[k] + \dfrac{u_1T_s}{L} \\ i_b[k+1] = (1 - \dfrac{RT_s}{L})i_b[k] + \dfrac{u_2T_s}{L} \\ i_c[k+1] = (1 - \dfrac{RT_s}{L})i_c[k] + \dfrac{u_3T_s}{L} \end{cases} \tag{3.3}$$

Where, in the control algorithm, $i_a[k]$ is evaluated as the measured current of phase A at the sample k and $i_a[k+1]$ is evaluated as the predicted value of the current of phase A at the sample k + 1.

3.4 Cost Function

In this chapter, the objective of the current control scheme is typically to minimize the error between the measured currents and the reference values. This objective can be mathematically formulated using a cost function. The cost function is defined as:

$$J = |i_a[k+1] - i_a^*[k+1]| + |i_b[k+1] - i_b^*[k+1]| + |i_c[k+1] - i_c^*[k+1]| \tag{3.4}$$

where $i_a^*[k+1], i_b^*[k+1] and i_c^*[k+1]$ are the reference values of the phase currents at the sample k+1.

3.5 MPCC working principle

Model Predictive Current Control (MPCC) regulates the output current of a power electronics system, such as a converter, in an accurate and efficient manner. The control algorithm aims to track a desired reference current while considering system constraints and optimizing control actions.

The MPC algorithm begins with measuring the current and evaluating the model for the first switching state to generate predicted variables. The cost function utilizes these variables to decide whether to keep or discard the switching state. This evaluation is repeated for all states, and the chosen state is then applied to the converter.

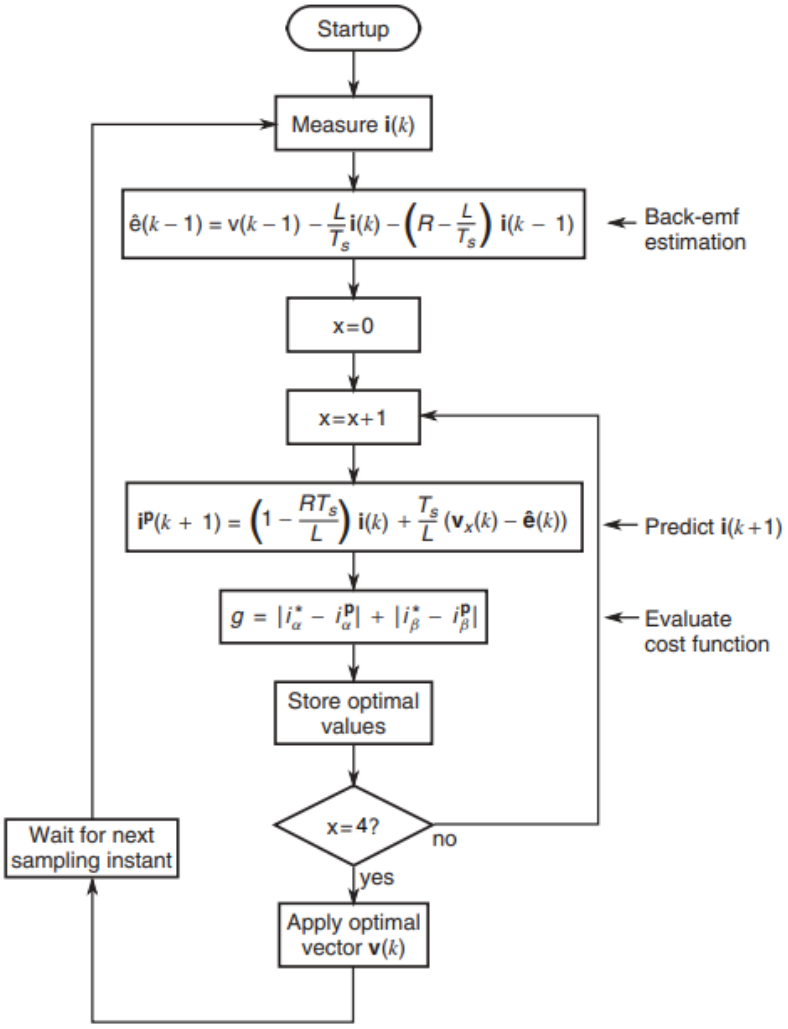

FIGURE 3.1: Flow diagram of MPCC

The MPCC scheme uses a finite number of valid switching states of the inverter in order to find the x_opt by using the following steps:

1. Measure the controlled variable $i[k]$ and estimate $i^*[k+1]$.

2. Apply the optimal switching state (computed in the previous sampling period) to calculate the output voltage of the inverter $v[k]$ using the inverter model.

3. For every switching state of the converter, predict (using the mathematical model) the behavior of current in the next sampling interval $i[k+1]$.

4. Evaluate the cost function or error, for each prediction as, for instance:

$$J = |i[k+1] - i^*[k+1]| \tag{3.5}$$

5. Select the switching state that minimizes the cost function, S_{opt}, and store it so that it can be applied to the converter in the next sampling period

3.6 Implementation of the MPCC strategy

In implementation, the currents and the output voltage of the inverter should be expressed in $\alpha\beta$ coordinate system, to simplify and minimize the computation time as follows:

$$\begin{cases} v = \dfrac{2}{3}(v_a + av_b + a^2 v_c) \\ i = \dfrac{2}{3}(i_a + ai_b + a^2 i_c) \end{cases} \tag{3.6}$$

where:

$$a = \exp\left(\frac{j2\pi}{3}\right) = -\frac{1}{2} + j\frac{\sqrt{3}}{2}$$
$$i_\alpha = Re(i)$$
$$i_\beta = Im(i)$$

Instead of calculating the output voltage of the inverter for each possible switching state at every iteration, we can calculate them in advance and apply them to the load model.

In order to reduce the number of calculations for the output current, we can transform the three equations into one equation using. We obtain:

$$i[k+1] = (1 - \frac{RT_s}{L})i[k] + \frac{vT_s}{L} \tag{3.7}$$

Thus, the cost function becomes:

$$J = |i[k+1] - i^*[k+1]| \tag{3.8}$$

The output voltage vectors of the inverter are stored and selected rather than calculated for each sampling period of the algorithm. The calculation of the cost function is a subtraction of two one-dimensional complex variables rather than three-dimensional variables. So, the number of calculations is considerably reduced.

3.7 Simulation Results and Analysis

To verify the proposed control strategy (model predictive current control), we used MATLAB (R2023a)/SIMULINK software components to implement the SIMULINK model given in Appendix C.

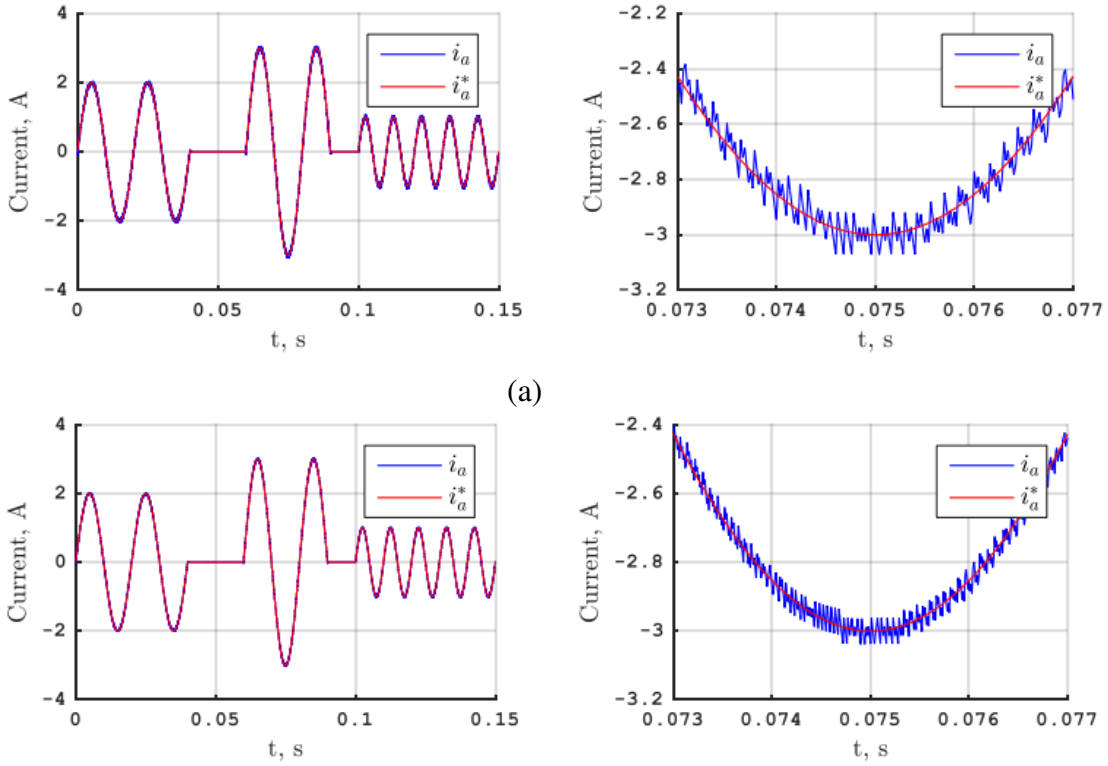

FIGURE 3.2: Simulation results of MPCC of a FSTP inverter-fed RL load: Reference and output current of phase A and their zoom with a sampling frequency of: (a) 50 KHz, (b) 100 KHz

Figure 3.2, Figure 3.3, Figure 3.4, Figure 3.5, Figure 3.6, Figure 3.7, and Figure 3.8 present the simulation results of the MPCC of a FSTP inverter-fed RL-load.

Figure 3.2 demonstrates that the output current effectively follows the reference in terms of magnitude, frequency, and phase, with a quick response time. However, there is a noticeable ripple or band around the reference due to oscillations in the output current. To minimize these oscillations, the sampling frequency can be increased, although this is not desirable for the power switches and controller circuit.

In Figure 3.3 and Figure 3.4, the output current and output voltage spectra are displayed as percentages of the fundamental magnitude, while keeping the reference frequency and magnitude constant. Notably, it is observed that the total harmonic distortion (THD) of the output current decreases as the sampling frequency increases.

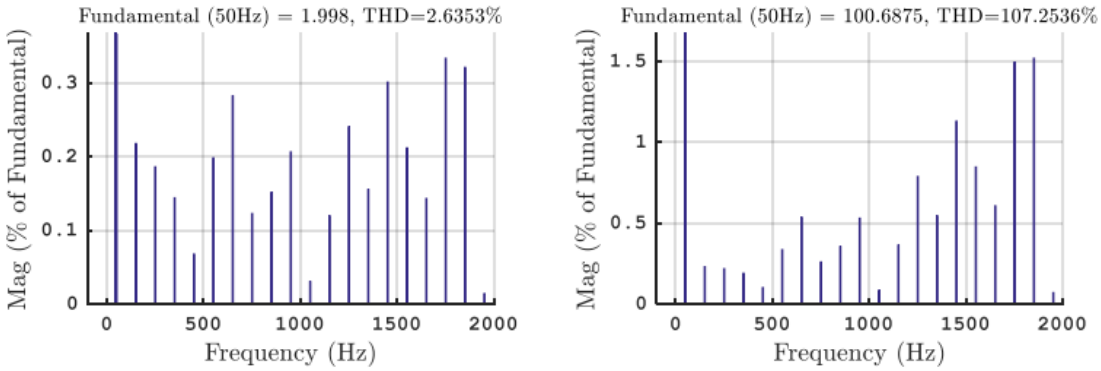

FIGURE 3.3: Simulation results of MPCC of a FSTP inverter-fed RL load: Output current and output voltage spectra expressed as percentages of fundamental magnitude, $|I^*| = 2Aandf^* = 50Hz$ with a sampling frequency of 50 KHz

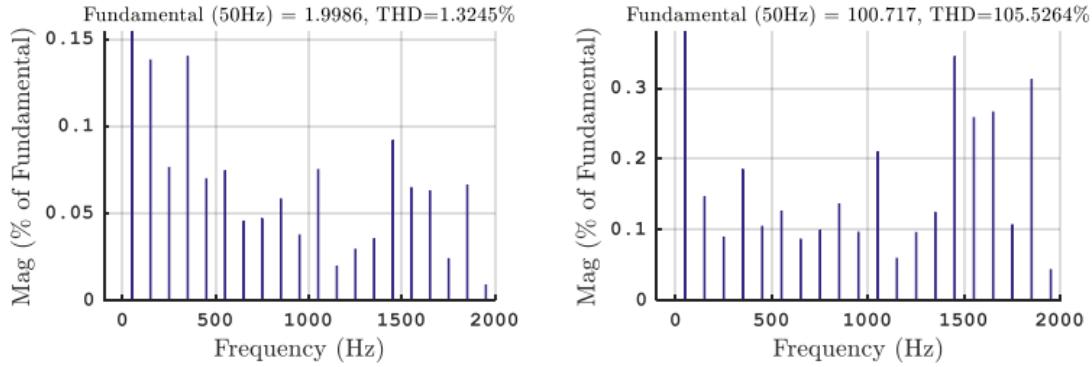

FIGURE 3.4: Simulation results of MPCC of a FSTP inverter-fed RL load: Output current and output voltage spectra expressed as percentages of fundamental magnitude, $|I^*| = 2Aandf^* = 50Hz$ with a sampling frequency of 100 KHz

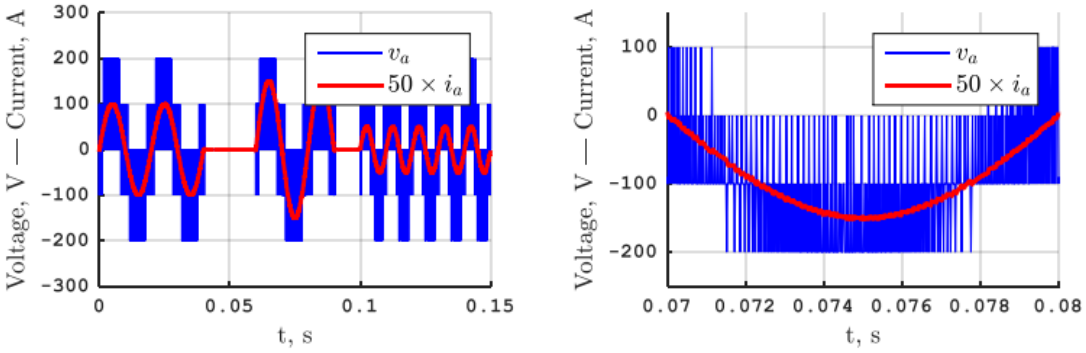

FIGURE 3.5: Simulation results of MPCC of a FSTP inverter-fed RL load: Output voltage of the inverter and 50 X the load current of phase A with a sampling frequency of 50 KHz

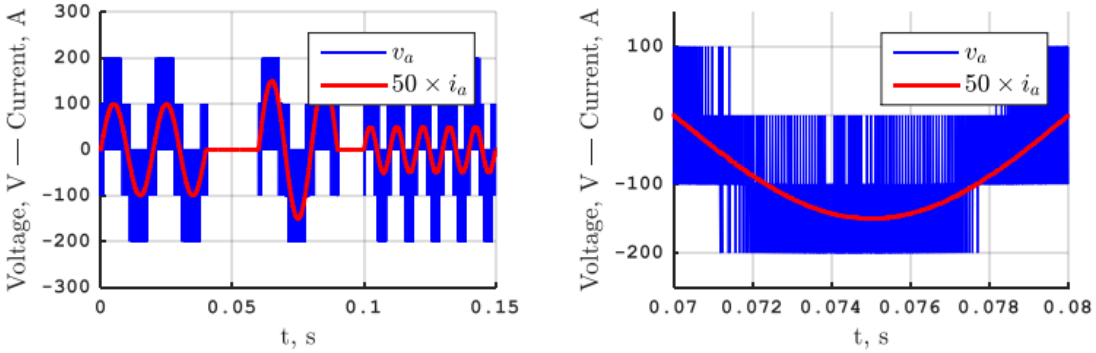

FIGURE 3.6: Simulation results of MPCC of a FSTP inverter-fed RL load: Output voltage of the inverter and 50 X the load current of phase A with a sampling frequency of 100 KHz

Figure 3.5 and Figure 3.6 depict the output voltage of the inverter and its spectra. The figure reveals a high total harmonic distortion (THD) in the output voltage. Furthermore, there is an observed phase shift between the output current and the output voltage, which can be attributed to the inductive characteristics of the RL-load.

3.8 Conclusion

In this chapter, the predictive current control strategy was introduced, both the converter and the load have been modelled and a cost function has been expressed. The MPCC working principle was explained in detail.

The control scheme was simulated in MATLAB/Simulink environment for different sampling frequencies and different references. The load current manages to track its reference and its quality gets better with high sampling frequencies (low THD).

The higher sampling frequencies help reduce the ripples of the output current, the error between the reference value and the output value of the load current in steady-state got reduced.

The inverter is controllable in both magnitude and frequency of the output current.

Even though the MPC can work with non-linear loads, it requires at least one derivative or integral in the load model in order to predict the value of the controlled variable.

MPCC of an RL-load is one of the simplest predictive control schemes. It allows us to apply this control scheme to other loads, like an induction machine for example, which is the subject of the following chapter.

Chapter 4

Model Predictive Torque Control of a FSTP Inverter-Fed Induction Motor

4.1 Introduction

Induction machines are known for their nonlinear nature, which complicates their control. However, the Model Predictive Torque Control (MPTC) strategy has emerged as a drive control technique for induction machines. MPTC offers benefits such as fast dynamic response, simple implementation, and robustness to rotor parameter variations.

In this chapter, the proposed Model Predictive Torque Control (MPTC) scheme has been applied to the system (inverter + machine), which is one of the most common electrical motor drive.

4.2 Model Predictive Torque Control

The stator flux (s) and electromagnetic torque (T) of an induction machine can be adjusted by carefully selecting a voltage vector sequence. This sequence allows for the manipulation of the stator flux magnitude and the variation of the angle between the rotor and stator flux. These principles are the foundation of direct torque control.

Predictive Torque Control (PTC) utilizes a similar principle, but with the addition of predicting future values for the stator flux and torque. In this scheme, a cost function is employed to determine the optimal reference condition, taking into account the anticipated behavior of these variables. Predictions are computed for each potential actuating scenario, and the cost function selects the voltage vector that optimizes the desired reference tracking. A block diagram of PTC shown in Figure 4.1 would visually represent this process.

4.3 Cost Function

MPC aims to minimize deviations between actual torque and flux values and their reference values, while reducing ripple. It involves selecting a voltage vector to drive system variables close to desired references. The cost function, typically based on absolute error, expresses the objective of MPC. As a result, the cost function can be

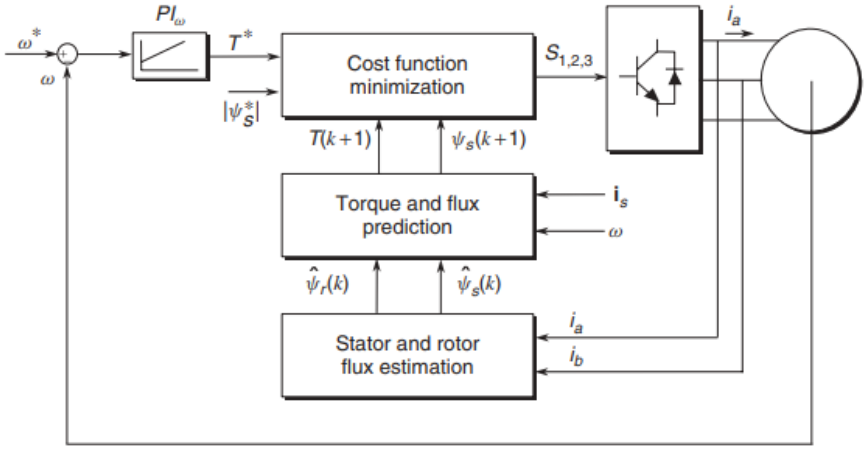

FIGURE 4.1: PTC scheme

expressed as:

$$J = \frac{|T^p_{e\,m} - T^*|}{T_{nom}} + \frac{|\phi^p_s - \phi^*_s|}{\phi_{s.nom}} \tag{4.1}$$

where:

1. $T^p_{e\,m}$: the predicted value of the electromagnetic torque
2. T^*: the reference value of the electromagnetic torque
3. T^{nom}: the nominal value of the electromagnetic torque
4. ϕ^p_s: the predicted value of the stator flux
5. ϕ^*_s: the reference value of the stator flux
6. $\phi_{s.nom}$: the nominal value of the stator flux

4.4 Working Principle

The working principle of the MPTC is summarizedin. At each instant KT_s, the future values of the state variables (the stator currenti_s and the rotor flux vectors ϕ_r) of the system are predicted for the instant (K+1)T_s using the system model, the measurements and necessary estimations. The optimal actuation is selected by the cost function and then applied to the inverter.

The following figure represents a flow diagram of the working principle of the MPTC. It uses finite number of valid switching states of the inverter in order to find the x_{opt} by using the following steps:

1. measurements of the stator currents and estimation of the stator flux and rotor flux.

2. For each valid switching state, apply the corresponding voltage vector.
3. Predict the values of the electromagnetic torque and statorflux of the next sampling period (k+1)T_s by applying the voltage vector $v_s[k]$ to the load model.
4. Evaluate the cost function by comparing the predicted values with their respective references and select the switching state that corresponds to the minimum value of the cost function.
5. Apply the optimal switching state x_{opt} to the inverter.

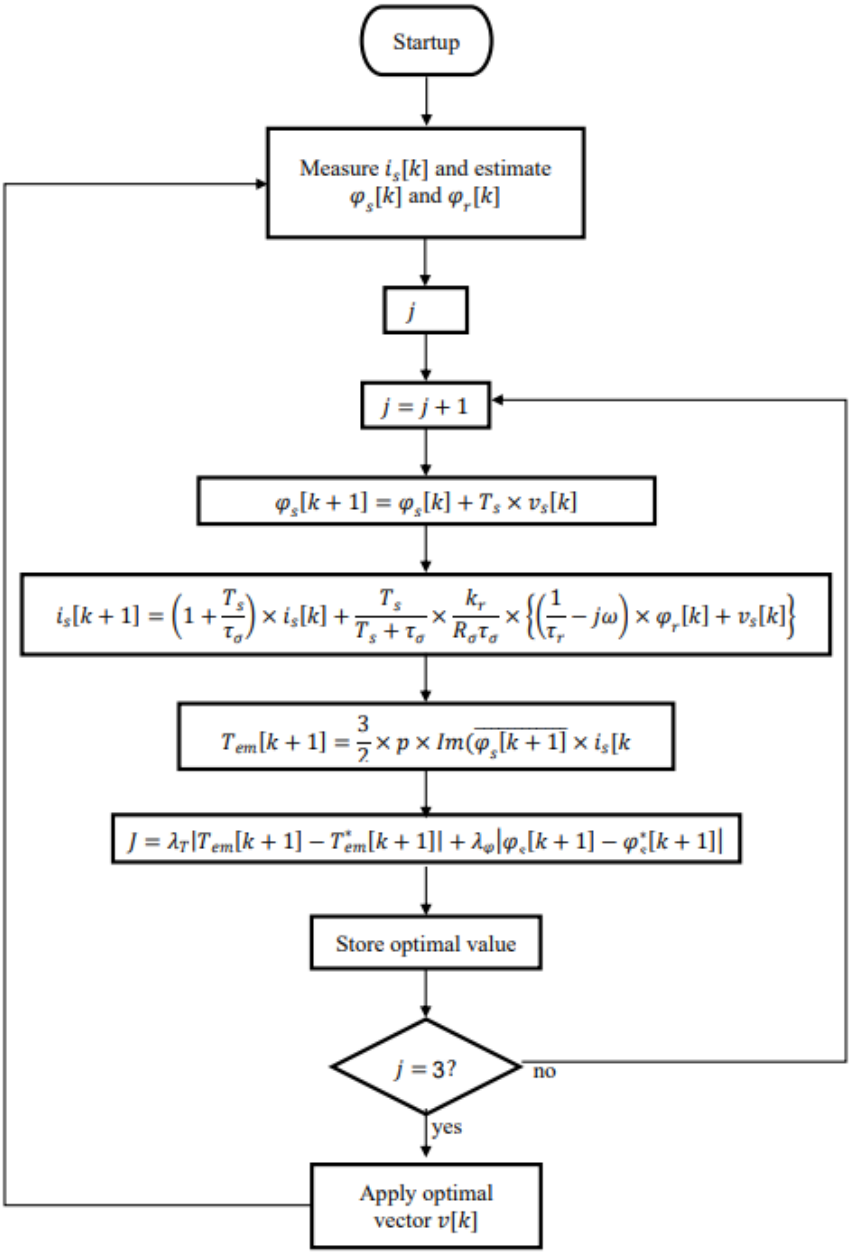

FIGURE 4.2: Flow diagram of the MPTC

4.5 Implementation

Due to the discrete nature of digital controllers, probably the most common and simple method to obtain a discrete-time representation for a continuous-time system is the Euler approximation of time derivatives. The obtained model corresponds to a first order Taylor expansion.

Choosing the stationary reference frame, w_k= 0, eliminates both multipliers in the internal feedback loops of the rotor winding and the stator winding.

After discretization and some arrangements of equations (2.7), (2.8), (2.9), and (2.10) mentioned in Chapter 2, we get:

We introduce the weighting factors λ_T and λ_ϕ

Where:

$$\lambda_T = \frac{1}{T_{nom}} and \lambda_\phi = \frac{1}{\phi_{s.nom}}$$

The cost function, thus, becomes:

$$J = \lambda_T |T_{em}[k+1] - T_{ref}| + \lambda_\Phi |\phi_{em}[k+1] - \phi_{s.ref}| \tag{4.2}$$

The model used to estimate the stator flux is derived from the equation (2.9), given that the reference frame is stationary we get:

$$\frac{d\phi_s}{dt} = v_s - R_s i_s \tag{4.3}$$

We can estimate the rotor flux ϕ_r by replacing i_r by its expression from (2.7) in (2.8), we get:

$$\phi_r = \frac{L_r}{L_m}\phi_s + (L_m - \frac{L_r L_s}{L_m}) i_s \tag{4.4}$$

As shown in Figure 4.3,the Proportional-Integral (PI) controller receives the error signal of the mechanical speed and computes the torque reference for the predictive controller.

By transforming (2.11) to Laplace domain we get:

$$\frac{W}{T_{em} - T_l} = \frac{1}{Js + k_f} \tag{4.5}$$

Where: s is the Laplace operator

By considering the load torque T_L as a nil disturbance, the transfer function (4.5),

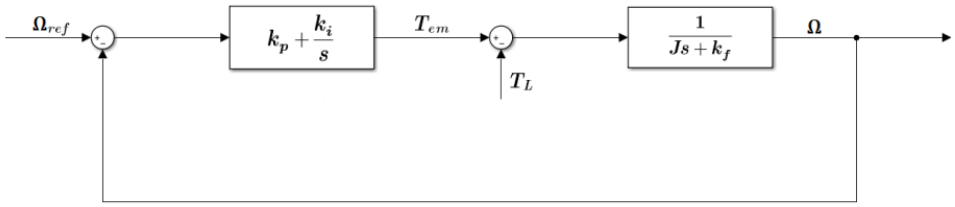

FIGURE 4.3: PI speed controller

in closed loop, becomes:

$$W = \frac{k_p}{J} X \frac{s + \frac{k_i}{k_p}}{s^2 + \frac{k_p + k_f}{J} s + \frac{k_i}{J}} W_{ref}$$

The denominator of (4.2) is a second order system of the form:

$$s^2 + 2\xi w_n s + w_n^2 \tag{4.6}$$

By identification we get:

$$k_i = J w_n^2 \tag{4.7}$$

$$k_p = 2\xi w_n - k_f \tag{4.8}$$

where:

ξ: damping coefficient

w_n: natural circular pulse

4.6 Simulation Results and Analysis

The MPTC technique was simulated with an Induction Machine fed by a FSTP inverter. The MPTC has been simulated in the MATLAB/Simulink environment with different values of the speed reference and the load torque.

The simulation employs the parameters outlined in Table D.1 and Table D.2, found in Appendix D. We examine two scenarios. Initially, we simulate the control scheme disregarding the stator flux limitation. Conversely, in the second scenario, we incorporate the prioritization of stator flux control over electromagnetic torque in the cost function as a flexible restriction.

Regarding the stator flux reference, it is set close to its nominal value of 0.82 Wb. The desired torque is generated through an external PI regulator loop.

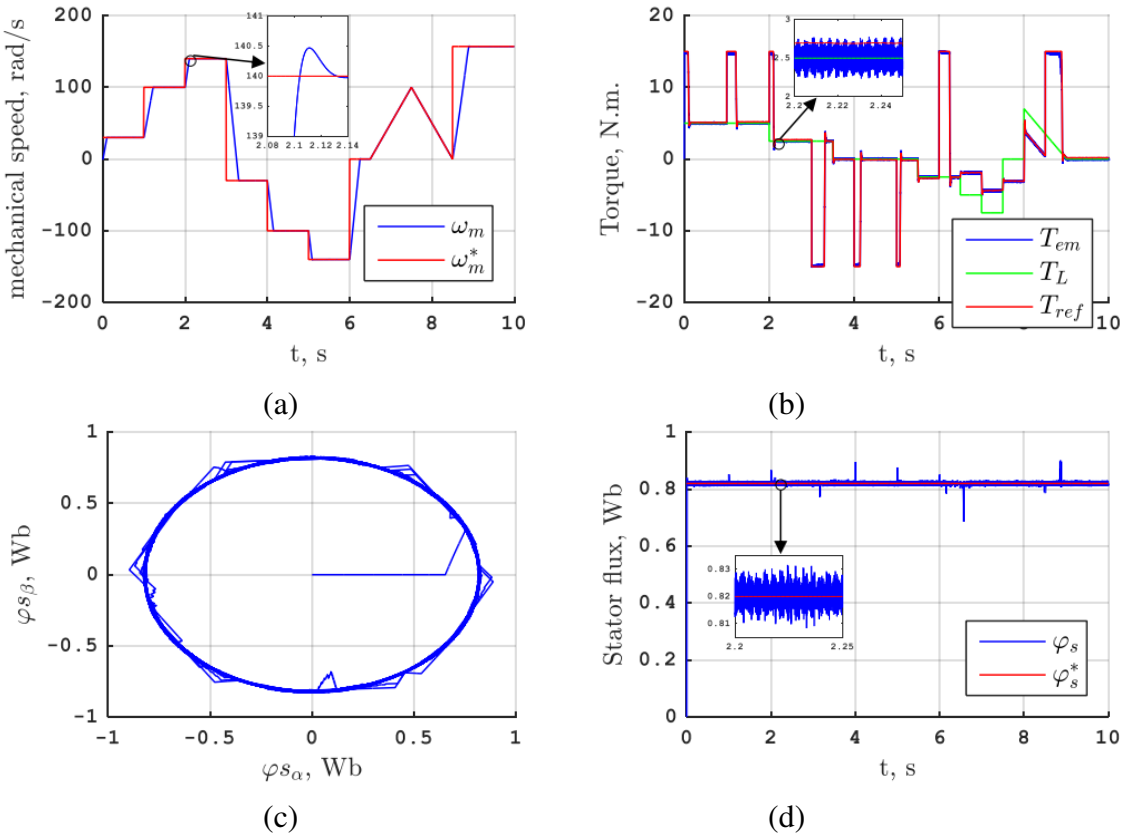

FIGURE 4.4: Simulation results of MPTC of a FSTP inverter-fed induction motor without prioritizing the control of the stator flux: (a) rotor speed and its reference, (b) electromagnetic, load and reference torque, (c) stator flux, (d) stator flux

The simulation results of the Model Predictive Torque Control (MPTC) for a 1.5 kW squirrel-cage induction machine, powered by an FSTP inverter, are depicted in Figure 4.4 and Figure 4.5 In this simulation, the prioritization of stator flux control is not enforced.

The induction motor starts at t = 0.0059 s with a slight reverse response in speed due to a load torque of 5 N.m. This negative speed is caused by the mentioned torque. Subsequently, the mechanical speed and electromagnetic torque follow their respective references.

1. At t = 0 s, the speed reference is set to 30 rad/s and it takes the motor 0.0972s to reach that setpoint. This response time could be reduced if the electromagnetic torque hadn't been limited to 15 N.m by the PI controller;

2. At t = 1 s, the speed reference is set to 100 rad/s with the same load torque;

3. At t = 2 s, although the load torque has decreased, the electromagnetic torque is at its peak value in order to get to rotor speed to 140 rad/s;

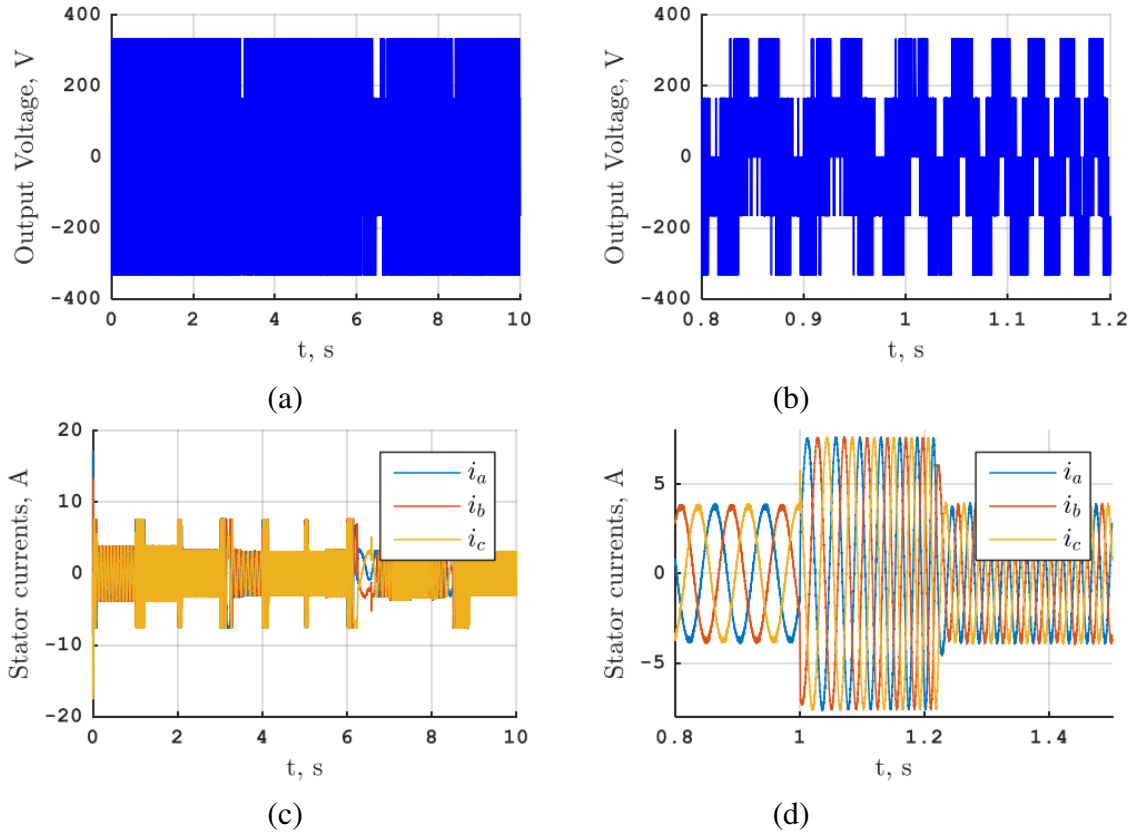

FIGURE 4.5: Simulation results of MPTC of a FSTP inverter-fed induction motor without prioritizing the control of the stator flux with a sampling frequency of 50 kHz: (a,b) output voltage of one phase of the inverter and its zoom, (c,d) stator currents and their zoom

4. At t 3 s, the speed reference has been reversed resulting in a negative electromagnetic torque, which is also limited by the PI controller to -15 N.m, until the moment the rotor reaches its reference -30 rad/s;

5. At t = 6.5 s, a linear increase in the speed reference is set up to 100 rad/s followed by linear decrease to 0 rad/s at t = 7.5 s;

6. The changes in the load torque value affect the speed but the PI controller compensates for that disturbance with a slight overshoot, which is due to the nature of the controller;

7. At t = 8.5 s, the speed is set to its nominal value, which is 157 rad/s.

Figure 4.4(a) shows that the mechanical speed follows its reference despite the variations of the load torque (and thus the reference torque) with a very small overshoot.

Figure 4.4(b) shows that the electromagnetic torque follows its reference and oscillates around the load torque. Same thing for the stator flux magnitude, it follows and oscillates around its reference with certain spikes during the transient states of the electromagnetic torque as shows Figure 4.4(d).

Figure 4.5 presents the results of the electric variables using MPTC. It shows that the frequency of these variables depends on the rotor speed. It also shows that the variations in the magnitude of the stator currents depend on the electromagnetic torque.

Figure 4.6 and 4.7 showcases the simulation results of the Model Predictive Torque Control (MPTC) for a 1.5 kW squirrel-cage induction machine powered by a FSTP inverter, with a focus on controlling the stator flux.

Comparing two cases, there is no significant difference in mechanical speed (Figure 4.4(a) and Figure 4.6(a)), but the second case with a higher value of X demonstrates improved stator flux performance (Figure 4.4(d) and Figure 4.7(b)).

The flux magnitude in the second case exhibits narrower oscillations around the reference compared to the first case. However, this improvement comes at the expense of electromagnetic torque quality, as indicated by Figure 4.4(b) and Figure 4.6(b). The first case has lower torque ripple at steady-state (0.4113 N.m) compared to the second case (0.4745 N.m).

To assess the stator current quality in relation to switching frequency, a simulation is conducted with the nominal speed set as reference and a load torque of 5 N.m.

Figure 4.8 and Figure 4.9 presents the simulation results of the stator currents for a FSTP inverter-fed induction machine using MPTC, along with their spectra at different sampling frequencies. Higher sampling frequencies tend to enhance the quality of the stator currents, with the machine windings acting as a filter for high-frequency harmonics.

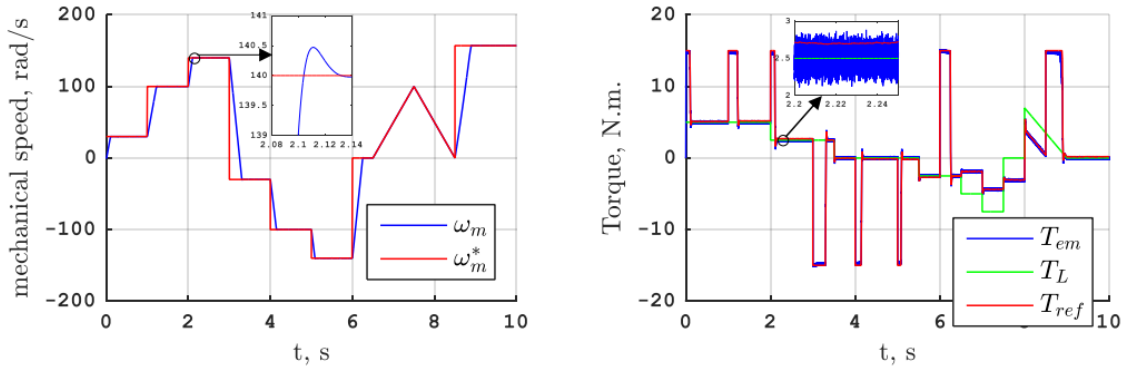

(a) (b)

FIGURE 4.6: Simulation results of MPTC of a FSTP inverter-fed induction motor with prioritizing the control of the stator flux: (a) rotor speed and its reference, (b) electromagnetic, load and reference torque

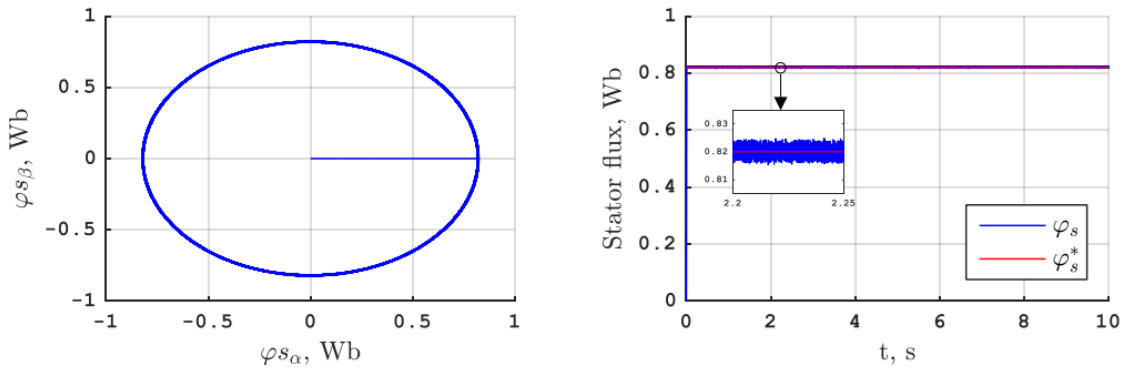

(a) (b)

FIGURE 4.7: Simulation results of MPTC of a FSTP inverter-fed induction motor with prioritizing the control of the stator flux: (a) stator flux, (b) reactive power

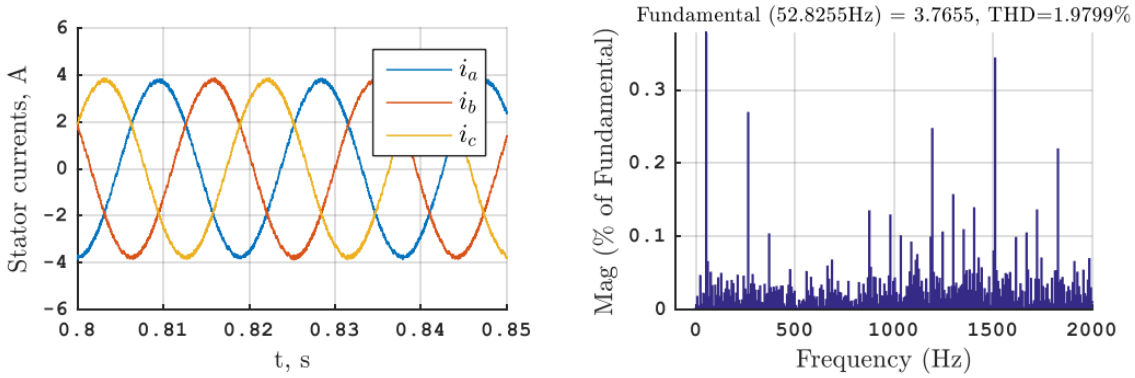

(a) (b)

FIGURE 4.8: Simulation results of the stator currents of an inverter-fed induction machine using MPTC and their spectra with a sampling frequency of 50 KHz

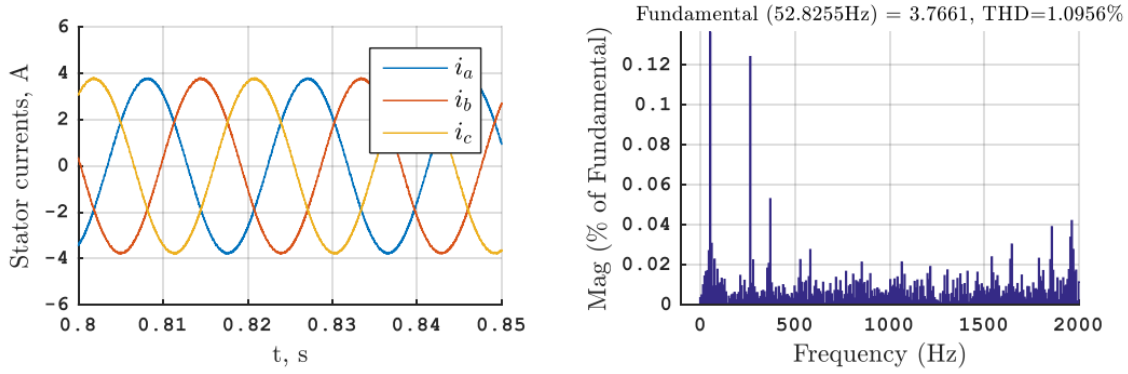

(a) (b)

FIGURE 4.9: Simulation results of the stator currents of an inverter-fed induction machine using MPTC and their spectra with a sampling frequency of 100 KHz

4.7 Comparison between MPC and DTC

Direct Torque Control (DTC) emerged as a novel approach in the 1980s, distinct from field-oriented control. It diverges from mathematical modeling and instead capitalizes on the physical dynamics of the machine and power supply. Through straightforward signal processing techniques, DTC harnesses the irregularities in the power source of variable speed drive systems.

4.7.1 Working Principle of DTC

Direct Torque Control (DTC) in AC drives offers simplified control schemes while achieving high dynamic performance for induction machines. DTC operates by utilizing independent set points for flux and torque. The control loop relies on estimated values of these quantities to establish closed-loop control.

Unlike vector control, DTC does not employ current controllers. Instead, two-level or three-level hysteresis controllers are used for torque and flux control. These controllers determine whether adjustments to flux and/or torque are required based on predefined error ranges. Using this information and knowledge of the stator flux linkage space vector's position, an appropriate voltage vector is selected using a switching strategy.

While an accurate knowledge of the stator flux linkage space vector's magnitude is necessary, the exact instantaneous position is not required. The control system only needs to determine the sector in the two-dimensional complex plane where the flux linkage space vector lies.

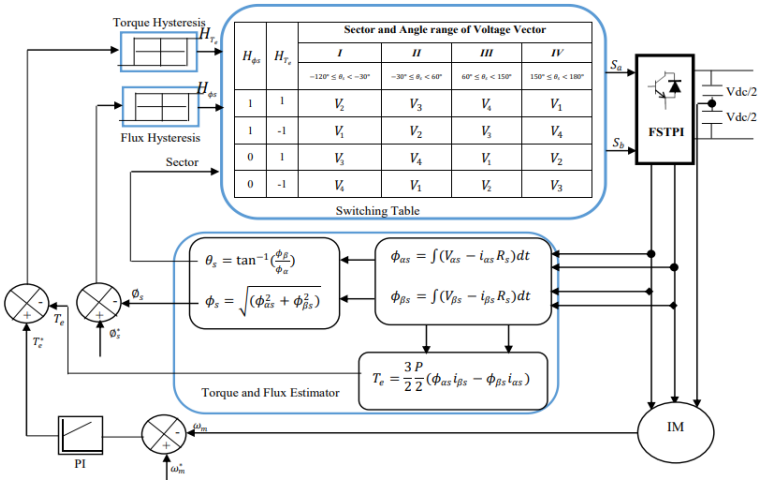

FIGURE 4.10: Block diagram of DTC with FSTP inverter

4.7.2 Simulation Results of DTC and Comparison

The DTC of a FSTP-fed induction machine is simulated in MATLAB/Simulink environment with the minimization of the input reactive power. The simulation parameters are the same as those applied previously.

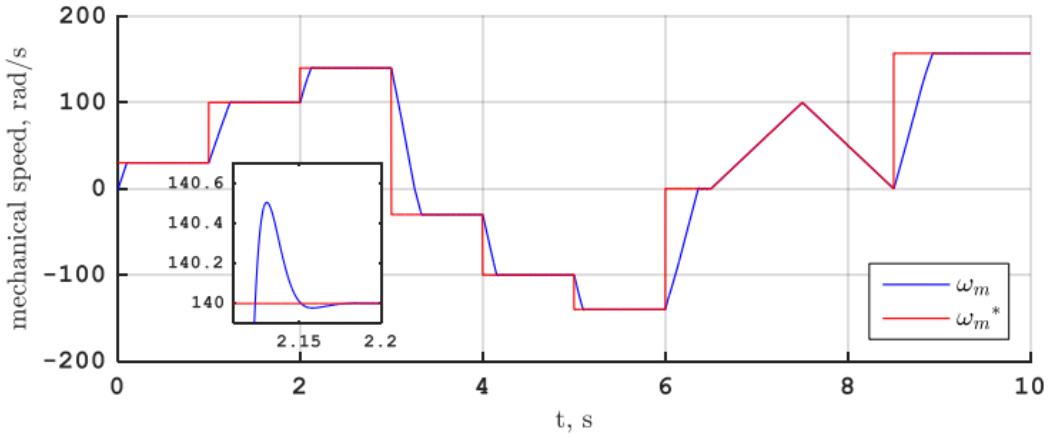

FIGURE 4.11: Simulation results of the DTC of a FSTP inverter-fed induction motor without the control of the input reactive power: rotor speed and its reference

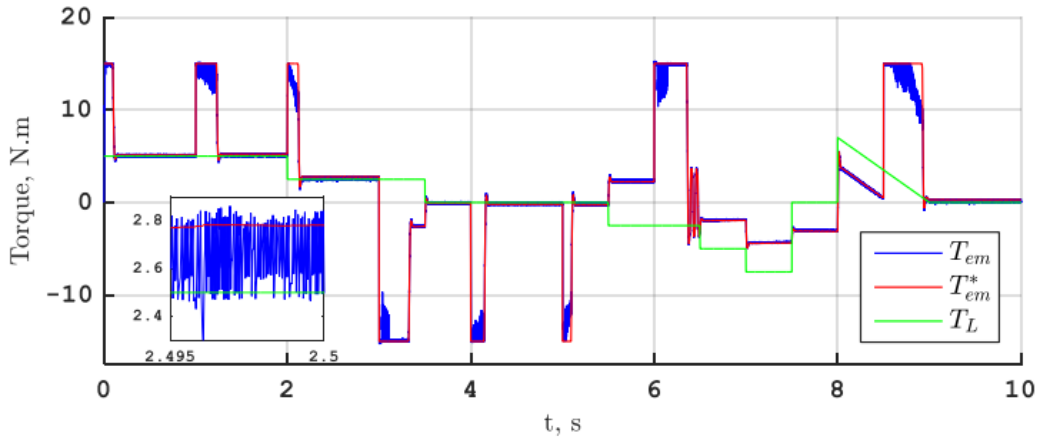

FIGURE 4.12: Simulation results of the DTC of a FSTP inverter-fed induction motor without the control of the input reactive power: electromagnetic, load, and reference torque

The results of applying DTC with PI speed regulation to a FSTP inverter-fed induction motor are summarized as follows:

- The speed closely follows its reference, which includes various scenarios such as constant speed, low, medium, and high speeds, speed inversion, and speed ramps. The response time is slightly longer than that of MPTC, with an additional delay of about 50 ms.
- The electromagnetic torque tracks the load torque during steady-state operation, but larger oscillations and a longer transient state are observed compared to MPTC.
- The stator flux follows its reference, although with increased oscillations. When the speed is in the form of a ramp, there is a slight divergence between the stator flux and stator current.

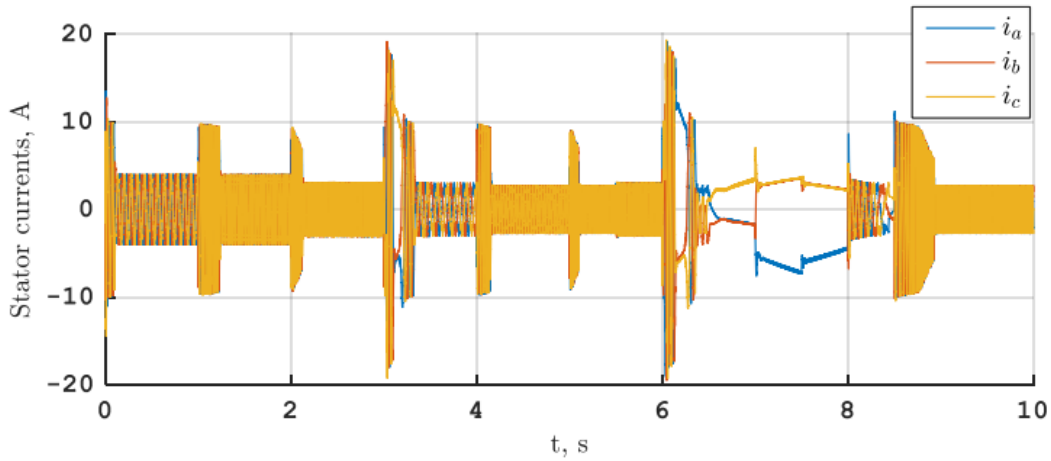

FIGURE 4.13: Simulation results of the DTC of a FSTP inverter-fed induction motor without the control of the input reactive power: stator currents

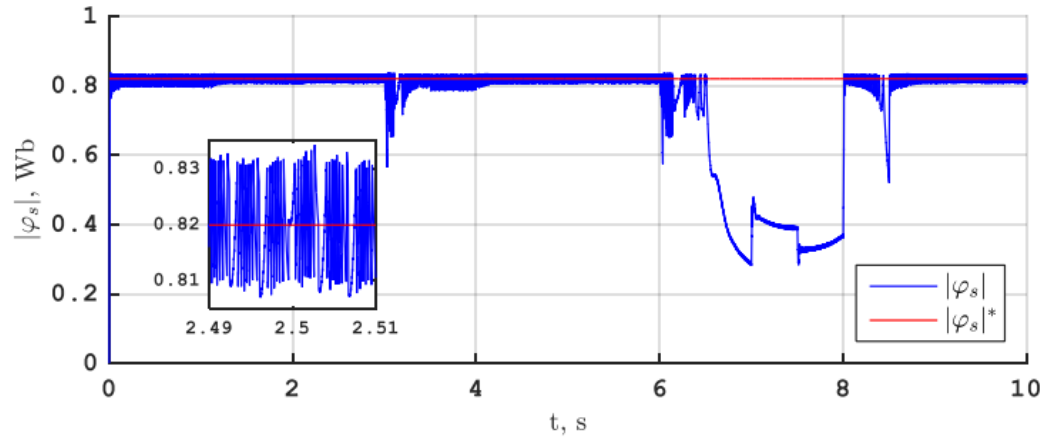

FIGURE 4.14: Simulation results of the DTC of a FSTP inverter-fed induction motor without the control of the input reactive power: stator flux

- Both the electromagnetic torque and stator flux stay within their respective hysteresis bands during steady-state operation, indicating successful control of these variables.

Contrary to MPTC, when the speed is reversed, spikes in the current and stator flux are observed.

When using DTC with a set point of 110 rad/s and 10 N.m, the mechanical speed, electromagnetic torque, and stator flux exhibit larger oscillations around their references compared to MPTC.

The stator current in DTC shows some distortion, whereas it is less distorted in MPTC. However, DTC offers improved waveforms for the stator voltage, supply current, and input current.

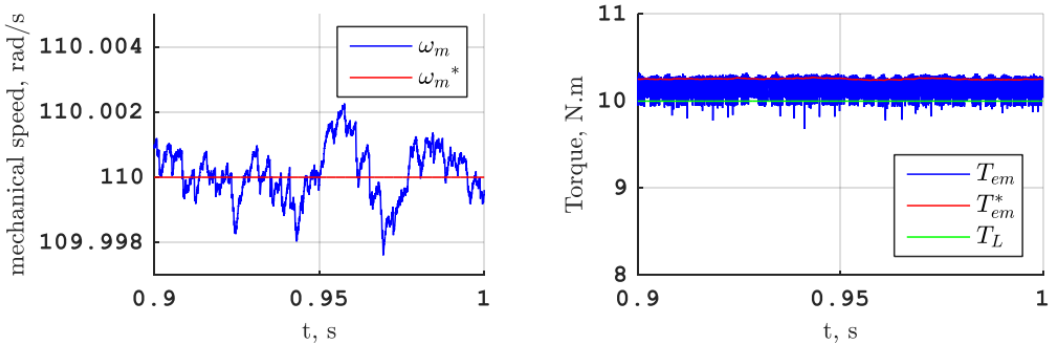

(a) (b)

FIGURE 4.15: Simulation results of the DTC of a FSTP inverter-fed induction motor with the control of the input reactive power: steady state of (a) mechanical speed and (b) electromagnetic torque

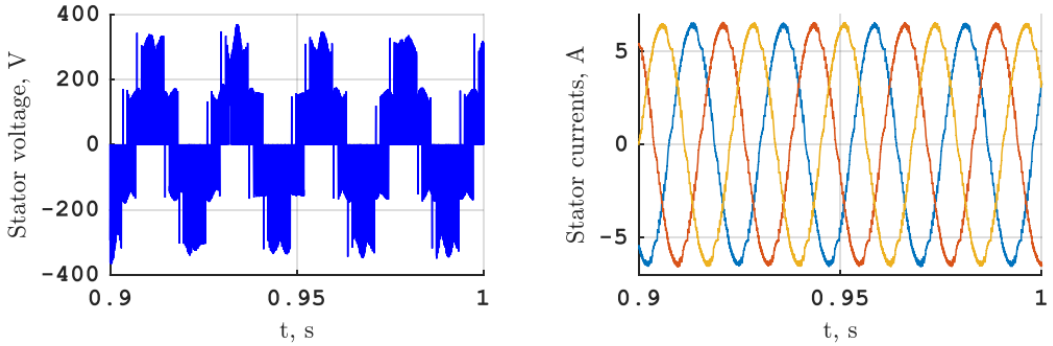

(a) (b)

FIGURE 4.16: Simulation results of the DTC of a FSTP inverter-fed induction motor with the control of the input reactive power: (a) stator voltage, (b) stator currents

In Summary:

1. Both DTC and MPTC methods require estimation of the stator flux, but DTC also requires estimation of the angle of the stator flux, whereas MPTC does not.

2. DTC necessitates both torque and flux hysteresis controllers, and tuning the hysteresis bands is crucial. This introduces two necessary parameters. In contrast, MPTC utilizes two weighting factors in the cost function, allowing for greater flexibility in handling constraints and balancing the importance of electromagnetic torque and flux control.

3. The transient response, as governed by the speed PI controllers, is the same for both methods. However, during the transient state, DTC exhibits higher torque ripples compared to MPTC, which demonstrates significantly lower ripple levels.

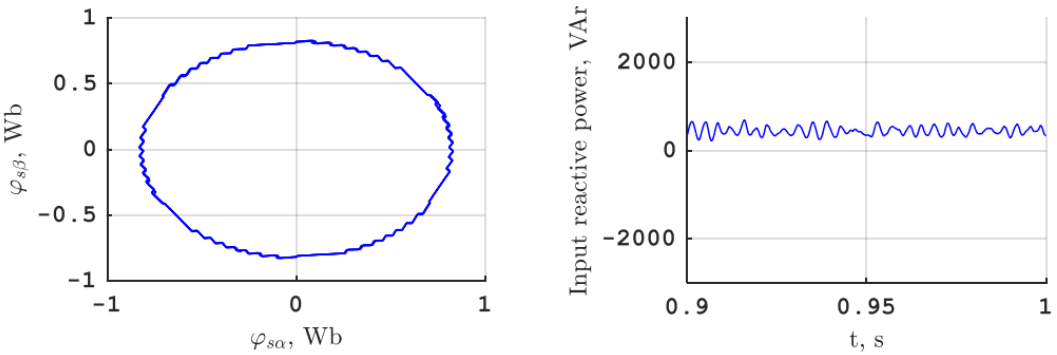

(a) (b)

FIGURE 4.17: Simulation results of the DTC of a FSTP inverter-fed induction motor with the control of the input reactive power: (a) stator flux, (b) input reactive power

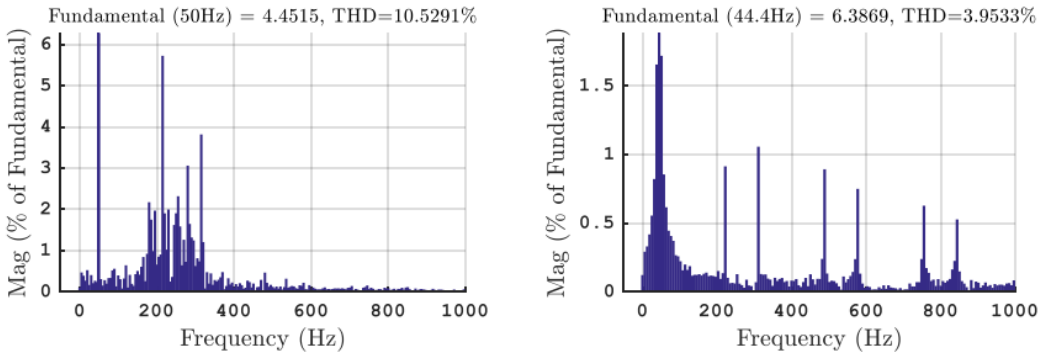

(a) (b)

FIGURE 4.18: Harmonic spectrum of (a) supply current, (b) stator current

4.8 Conclusion

In this chapter, the Model Predictive Torque Control (MPTC) was introduced for an induction motor fed by a FSTP inverter. The motor was modeled to suit the control scheme, and a cost function was defined to achieve the control objectives. The working principle of MPTC was explained in detail.

MATLAB/Simulink simulations were conducted with varying weighting factors to showcase one advantage of Model Predictive Control. The simulation results demonstrated the excellent performance and fast dynamics of this control strategy, comparable to traditional approaches like Direct Torque Control (DTC).

MPTC offers the flexibility to easily incorporate system constraints by tuning the weighting factors in the cost function. This allows for deciding the relative importance of the electromagnetic error signal versus the stator flux error signal, enhancing the control strategy's adaptability.

General Conclusion

In this work, Model Predictive Control (MPC) schemes were applied to a four-switch three-phase (FSTP) inverter with a RL load and an induction machine. The study was conducted through simulations in MATLAB/Simulink.

The first chapter provided a general description of the FSTP inverter, followed by an introduction to MPC, explaining its working principle and applications. attention.

In the second chapter, a comprehensive overview of induction motors, Variable Frequency Drives (VFDs), and voltage source inverters was presented. By establishing a solid understanding of induction motors, readers are better equipped to delve into the intricacies of VFDs and voltage source inverters in later chapters.

In the second chapter, the predictive current control strategy (MPCC) for FSTP inverter-fed RL-load was introduced. The MPCC demonstrated effective tracking of load current references, with improved quality achieved through high sampling frequencies (low Total Harmonic Distortion). The inverter, with the aid of MPCC, was able to control the output current in terms of magnitude and frequency.

The third chapter focused on the application of Model Predictive Torque Control (MPTC) to an induction motor fed by a FSTP inverter. The MPTC strategy showcased excellent performance and fast dynamics comparable to traditional approaches like Direct Torque Control (DMC). Additionally, MPTC offered flexibility by allowing system constraints to be easily included in the cost function through tuning of weighting factors.

The proposed control strategy demonstrates excellent performance in several aspects. Firstly, the mechanical speed tracks its reference accurately, even in the presence of load torque variations, which are considered as disturbances. This indicates the robustness of the control strategy in maintaining the desired speed.

Secondly, the average value of the electromagnetic torque closely follows the load torque in steady state, indicating effective torque control. Similarly, the stator flux also tracks its reference well, demonstrating successful flux control.

The control strategy exhibits flexibility by allowing the addition of soft constraints through the tuning of weighting factors. This enables fine-tuning and prioritization of control objectives according to specific requirements.

Furthermore, the stator current shows a low Total Harmonic Distortion (THD), indicating a good waveform and high-quality current output.

In the final part of this thesis, the performance of Model Predictive Torque Control (MPTC) is compared to Direct Torque Control (DTC), and it is shown that despite the computational power requirement, MPC yields superior results.

Despite the higher computational requirements, MPC proves to be superior in terms of overall results. The advantages of predictive control, including simplicity, the ability to handle multivariable cases, easy inclusion of constraints and nonlinearities, fast dynamics, and robustness, are highlighted.

Model Predictive Control emerges as a promising option for power converters and electrical drives. The future perspectives for Model Predictive Control (MPC) applied to a four-switch three-phase inverter fed induction motor include:

- Development of advanced control algorithms tailored for the specific characteristics of the four-switch three-phase inverter topology.
- Implementation of the MPC algorithm on dedicated hardware platforms like FPGAs or DSPs for real-time control and practical validation.
- Integration of fault detection and diagnosis algorithms to enhance system resilience and fault tolerance.
- Application of optimization techniques for model parameter identification and adaptation to further enhance MPC performance and efficiency.
- Consideration of energy management strategies and grid integration features to enable effective utilization of renewable energy sources and seamless integration with the electrical grid.

References

[1] M. S. Diab, A. Elserougi, A. M. Massoud, A. S. Abdel-Khalik and S. Ahmed, "A Four-Switch Three-Phase SEPIC-Based Inverter," in IEEE Transactions on Power Electronics, vol. 30, no. 9, pp. 4891-4905, Sept. 2015, doi: 10.1109/TPEL.2014.2363853.

[2] M. B. de Rossiter Correa, C. B. Jacobina, E. R. C. da Silva and A. M. N. Lima, "A General PWM Strategy for Four-Switch Three-Phase Inverters," in IEEE Transactions on Power Electronics, vol. 21, no. 6, pp. 1618-1627, Nov. 2006, doi: 10.1109/TPEL.2006.882964.

[3] B. El Badsi, B. Bouzidi and A. Masmoudi, "DTC Scheme for a Four-Switch Inverter-Fed Induction Motor Emulating the Six-Switch Inverter Operation," in IEEE Transactions on Power Electronics, vol. 28, no. 7, pp. 3528-3538, July 2013, doi: 10.1109/TPEL.2012.2225449.

[4] M. N. Uddin, T. S. Radwan and M. A. Rahman, "Fuzzy-logic-controller-based cost-effective four-switch three-phase inverter-fed IPM synchronous motor drive system," in IEEE Transactions on Industry Applications, vol. 42, no. 1, pp. 21-30, Jan.-Feb. 2006, doi: 10.1109/TIA.2005.861277.

[5] C. -T. Lin, C. -W. Hung and C. -W. Liu, "Position Sensorless Control for Four-Switch Three-Phase Brushless DC Motor Drives," in IEEE Transactions on Power Electronics, vol. 23, no. 1, pp. 438-444, Jan. 2008, doi: 10.1109/TPEL.2007.911782.

[6] K. D. Hoang, Z. Q. Zhu and M. P. Foster, "Influence and Compensation of Inverter Voltage Drop in Direct Torque-Controlled Four-Switch Three-Phase PM Brushless AC Drives," in IEEE Transactions on Power Electronics, vol. 26, no. 8, pp. 2343-2357, Aug. 2011, doi: 10.1109/TPEL.2010.2096561.

[7] R. Wang, J. Zhao and Y. Liu, "A Comprehensive Investigation of Four-Switch Three-Phase Voltage Source Inverter Based on Double Fourier Integral Analysis," in IEEE Transactions on Power Electronics, vol. 26, no. 10, pp. 2774-2787, Oct. 2011, doi: 10.1109/TPEL.2011.2119381.

[8] H. W. Van Der Broeck and J. D. Van Wyk, "A Comparative Investigation of a Three-Phase Induction Machine Drive with a Component Minimized Voltage-Fed Inverter under Different Control Options," in IEEE Transactions on Industry Applications, vol. IA-20, no. 2, pp. 309-320, March 1984, doi: 10.1109/TIA.1984.4504413.

[9] S. Dasgupta, S. N. Mohan, S. K. Sahoo and S. K. Panda, "Application of Four-Switch-Based Three-Phase Grid-Connected Inverter to Connect Renewable Energy Source to a Generalized Unbalanced Microgrid System," in IEEE Transactions on Industrial Electronics, vol. 60, no. 3, pp. 1204-1215, March 2013, doi: 10.1109/TIE.2012.2202350.

[10] M. B. de Rossiter Correa, C. B. Jacobina, E. R. C. da Silva and A. M. N. Lima, "A General PWM Strategy for Four-Switch Three-Phase Inverters," in IEEE Transactions on Power Electronics, vol. 21, no. 6, pp. 1618-1627, Nov. 2006, doi: 10.1109/TPEL.2006.882964.

[11] Model Predictive Control System Design and Implementation Using MATLAB®. London: Springer London, 2009. doi: 10.1007/978-1-84882-331-0.

[12] « Model Predictive Control by E. F. Camacho, C. Bordons (z-lib.org).pdf ».

[13] M. Grimble, « LQG predictive optimal control for adaptive applications », Automatica, vol. 26, no 6, p. 949-961, 1990.

[14] A. M. Dadu, S. Mekhilef, et T. K. Soon, « Lyapunov model predictive control to optimize computational burden, reference tracking and THD of three-phase four-leg inverter », IET Power Electron., vol. 12, no 5, p. 1061-1070, 2019.

[15] S. Vazquez et al., "Model Predictive Control: A Review of Its Applications in Power Electronics," in IEEE Industrial Electronics Magazine, vol. 8, no. 1, pp. 16-31, March 2014, doi: 10.1109/MIE.2013.2290138.

[16] J. Rodriguez et P. Cortes, Predictive control of power converters and electrical drives, vol. 40. John Wiley Sons, 2012.

[17] Y. Sun, W. Xiong, M. Su, X. Li, H. Dan, et J. Yang, « Topology and Modulation for a New Multilevel Diode-Clamped Matrix Converter », IEEE Trans. Power Electron., vol. 29, no 12, p. 6352-6360, déc. 2014, doi: 10.1109/TPEL.2014.2305711.

[18] R. E. Pérez-Guzmán, M. Rivera and P. W. Wheeler, "Recent Advances of Predictive Control in Power Converters," 2020 IEEE International Conference on Industrial Technology (ICIT), Buenos Aires, Argentina, 2020, pp. 1100-1105, doi: 10.1109/ICIT45562.2020.9067169.

[19] M. Khalid and S. Omatu, "A neural network based control scheme with an adaptive neural model reference structure," [Proceedings] 1991 IEEE International Joint Conference on Neural Networks, Singapore, 1991, pp. 2128-2133 vol.3, doi: 10.1109/IJCNN.1991.170702.

[20] J. Rodriguez et al., "State of the Art of Finite Control Set Model Predictive Control in Power Electronics," in IEEE Transactions on Industrial Informatics, vol. 9, no. 2, pp. 1003-1016, May 2013, doi: 10.1109/TII.2012.2221469.

[21] S. Borreggine, V. G. Monopoli, G. Rizzello, D. Naso, F. Cupertino and R. Consoletti, "A Review on Model Predictive Control and its Applications in Power Electronics," 2019 AEIT International Conference of Electrical and Electronic Technologies for Automotive (AEIT AUTOMOTIVE), Turin, Italy, 2019, pp. 1-6, doi: 10.23919/EETA.2019.8804594.

[22] E. Fernandez-Camacho et C. Bordons-Alba, Model Predictive Control in the Process Industry. London: Springer London, 1995. doi 10.1007/978-1-4471-3008-6.

[23] H. M. Basri, K. Lias and S. Mekhilef, "Digital Predictive Current Control Fed by Three-Level Indirect Matrix Converter under Unbalanced Power Supply Condition," 2019 International UNIMAS STEM 12th Engineering Conference (EnCon), Kuching, Malaysia, 2019, pp. 34-39, doi: 10.1109/EnCon.2019.8861266.

[24] M. Uddin, S. Mekhilef, M. Rivera and J. Rodriguez, "Predictive indirect matrix converter fed torque ripple minimization with weighting factor optimization," 2014 International Power Electronics Conference (IPEC-Hiroshima 2014 - ECCE ASIA), Hiroshima, Japan, 2014, pp. 3574-3581, doi: 10.1109/IPEC.2014.6870011.

[25] Qu Wenlong, Yang Yi and Feng Jianghua, "Control strategies of direct torque control of induction motor applied to traction," ICEMS'2001. Proceedings of the Fifth International Conference on Electrical Machines and Systems (IEEE Cat. No.01 EX501), Shenyang, China, 2001, pp. 1226-1229 vol.2, doi: 10.1109/ICEMS.2001.971903.

[26] S. Vazquez, J. Rodriguez, M. Rivera, L. G. Franquelo and M. Norambuena, "Model Predictive Control for Power Converters and Drives: Advances and Trends," in IEEE Transactions on Industrial Electronics, vol. 64, no. 2, pp. 935-947, Feb. 2017, doi: 10.1109/TIE.2016.2625238.

[27] M. Abdelrahem, Z. Zhang, R. Kennel, H. Eldeeb and C. Hackl, "Simple and robust direct-model predictive current control technique for PMSGs in variable-speed wind turbines," 2017 IEEE International Symposium on Predictive Control of Electrical Drives and Power Electronics (PRECEDE), Pilsen, Czech Republic, 2017, pp. 1-6, doi: 10.1109/PRECEDE.2017.8071099.

[28] M. Abdelrahem, C. Hackl, R. Kennel and J. Rodriguez, "Sensorless Predictive Speed Control of Permanent-Magnet Synchronous Generators in Wind Turbine Applications," PCIM Europe 2019; International Exhibition and Conference for Power Electronics, Intelligent Motion, Renewable Energy and Energy Management, Nuremberg, Germany, 2019, pp. 1-8.

[29] M. Parvez Akter, S. Mekhilef, N. Mei Lin Tan and H. Akagi, "Modified Model Predictive Control of a Bidirectional AC–DC Converter Based on Lyapunov Function for Energy Storage Systems," in IEEE Transactions on Industrial Electronics, vol. 63, no. 2, pp. 704-715, Feb. 2016, doi: 10.1109/TIE.2015.2478752.

[30] Akter, Md. Parvez, Saad Mekhilef, Nadia Mei Lin Tan and Hirofumi Akagi. "Model predictive control of bidirectional AC-DC converter for the energy storage system." Journal of Electrical Engineering Technology 10 (2015): 165-175.

[31] B. Stellato, T. Geyer and P. J. Goulart, "High-Speed Finite Control Set Model Predictive Control for Power Electronics," in IEEE Transactions on Power Electronics, vol. 32, no. 5, pp. 4007-4020, May 2017, doi: 10.1109/TPEL.2016.2584678.

[32] M. Uddin, S. Mekhilef, M. Rivera and J. Rodriguez, "Predictive indirect matrix converter fed torque ripple minimization with weighting factor optimization," 2014 International Power Electronics Conference (IPEC-Hiroshima 2014 - ECCE ASIA), Hiroshima, Japan, 2014, pp. 3574-3581, doi: 10.1109/IPEC.2014.6870011.

[33] L. Yan and X. Song, "Design and Implementation of Luenberger Model-Based Predictive Torque Control of Induction Machine for Robustness Improvement," in IEEE Transactions on Power Electronics, vol. 35, no. 3, pp. 2257-2262, March 2020, doi: 10.1109/TPEL.2019.2939283.

[34] W. C. Wong et J. H. Lee, « Postdecision-state-based approximate dynamic programming for robust predictive control of constrained stochastic processes », Ind. Eng. Chem. Res., vol. 50, no 3, p. 1389-1399, 2011.

[35] X. Liang, B. Cui and X. Lou, "Model predictive control based on recurrent neural network," Proceeding of the 11th World Congress on Intelligent Control and Automation, Shenyang, China, 2014, pp. 4835-4839, doi: 10.1109/WCICA.2014.7053532.

[36] F. Blaschke, "The principle of field-orientation applied to transvector closed-loop control system for rotating field machines," Siemens Review, vol. XXXIX, no. 5, pp. 217–219, 1972.

[37] I. Takahashi and T. Noguchi, "A New Quick-Response and High-Efficiency Control Strategy of an Induction Motor," in IEEE Transactions on Industry Applications, vol. IA-22, no. 5, pp. 820-827, Sept. 1986, doi: 10.1109/TIA.1986.4504799.

[38] B. El Badsi, B. Bouzidi and A. Masmoudi, "DTC Scheme for a Four-Switch Inverter-Fed Induction Motor Emulating the Six-Switch Inverter Operation," in IEEE Transactions on Power Electronics, vol. 28, no. 7, pp. 3528-3538, July 2013, doi: 10.1109/TPEL.2012.2225449.

Appendix A

Modelling of induction motor

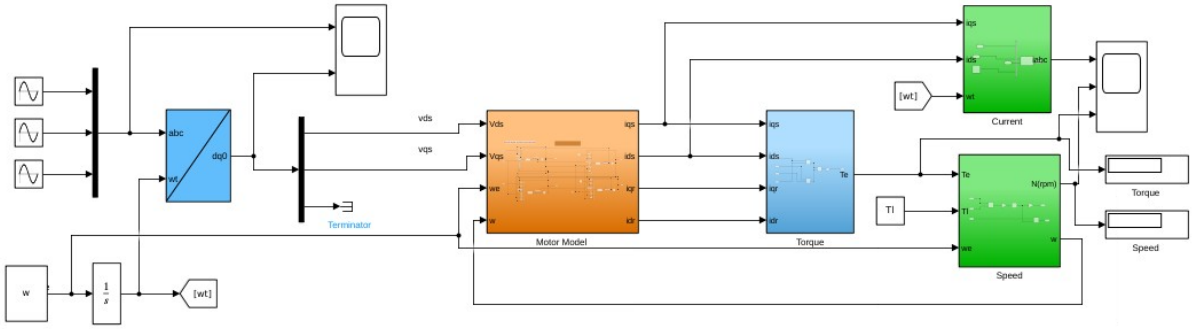

FIGURE A.1: Mathematical modeling of a three-phase induction motor

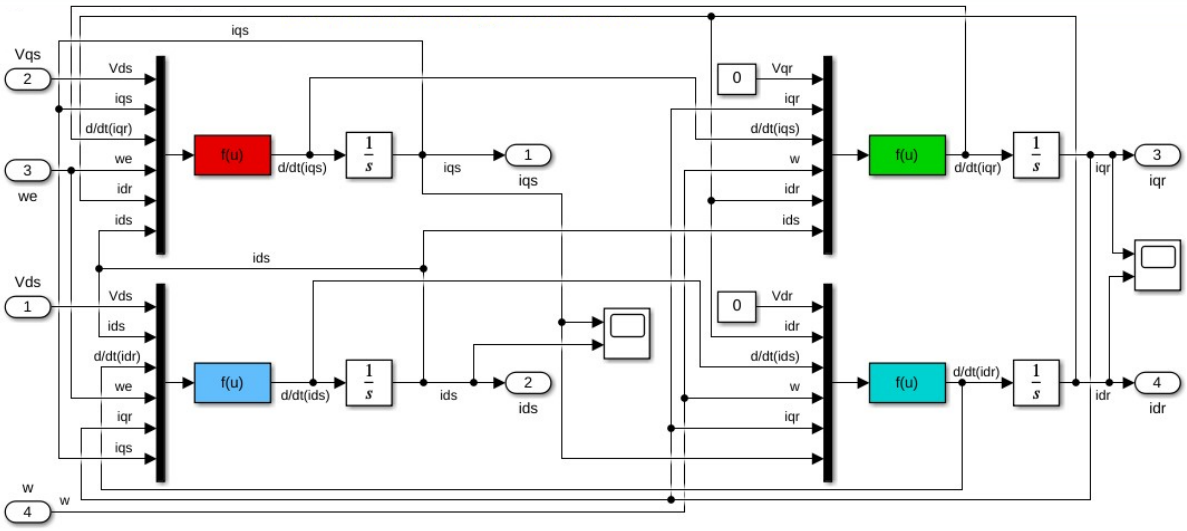

FIGURE A.2: Motor model

Appendix B

SVPWM for the FSTP inverter

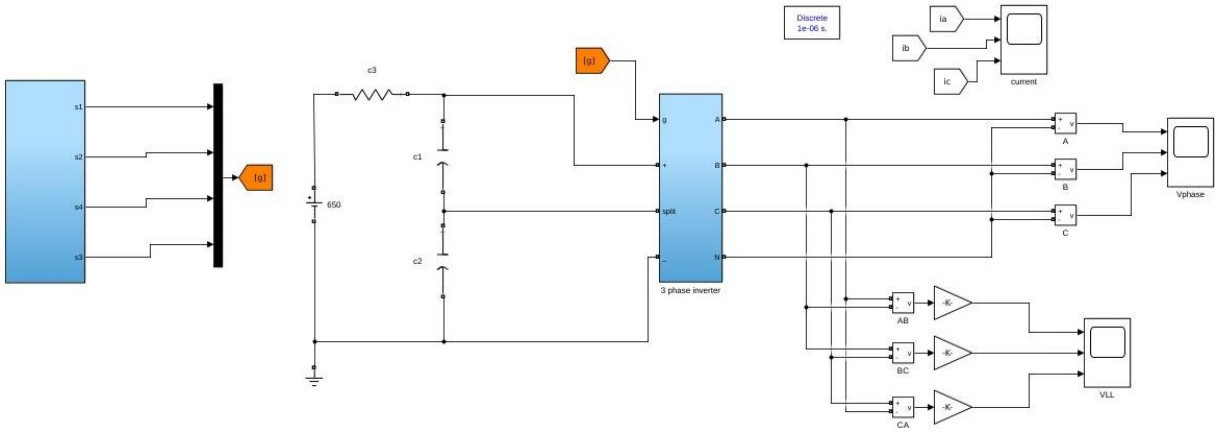

FIGURE B.1: Simulink model of SVPWM for the FSTP inverter

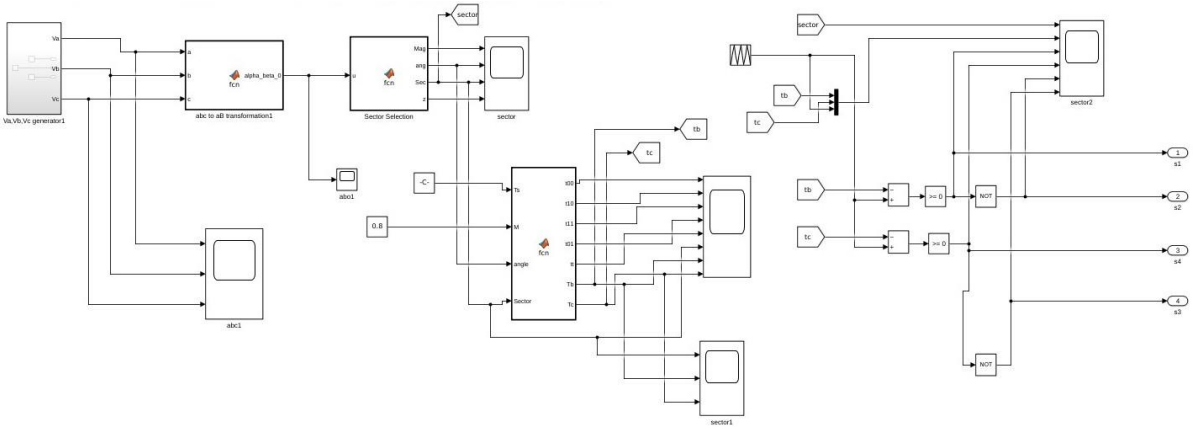

FIGURE B.2: Simulink model of SVPWM for the FSTP inverter

Appendix C

MPCC of FSTP inverter fed RL-load

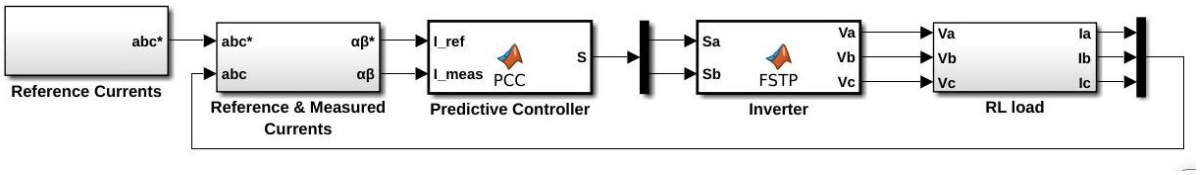

FIGURE C.1: Simulink model of the MPCC of FSTP inverter fed RL-load

TABLE C.1: Simulation parameters for the MPCC of FSTP inverter fed RL-load

Parameter	Value
Fixed-step size	5 μs
Solver	ode3
Tasking mode	SingleTasking
Resistance	50 Ω
Inductance	20 mH
DC voltage	300 V

Appendix D

MPTC of FSTP inverter fed induction motor

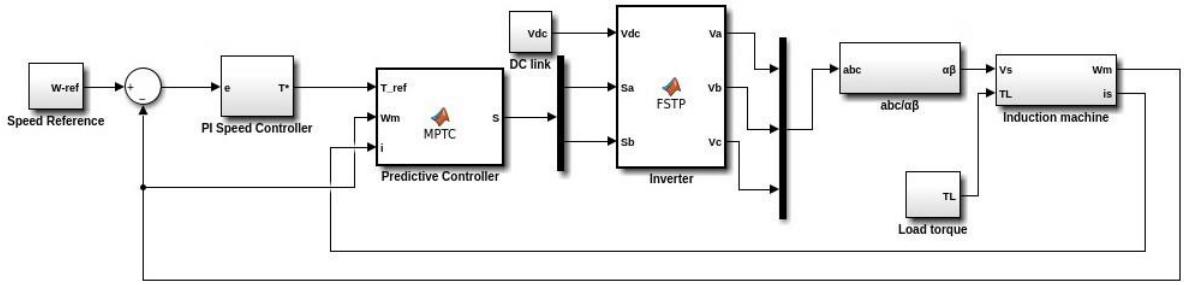

FIGURE D.1: Simulink model of the MPTC of FSTP inverter fed induction motor

TABLE D.1: Machine parameters

Description	Variables	Values
Rated power	P_{nom}	1.5 kW
Rated torque	T_{nom}	15 N.m
Rated speed	Ω_{nom}	157 rad/s
Rated stator current (RMS)	I_{nom}	6.7 A
Stator resistance	R_s	4.85 Ω
Stator inductance	L_s	0.274 H
Rotor resistance	R_r	6.3 Ω
Rotor inductance	L_r	0.274 H
Magnetizing inductance	L_m	0.258 H
Pole pairs	p	2
Dry friction coefficient	k_f	N.m.s.rad^{-1}
Moment of inertia	J	0.031 kg.m^2

TABLE D.2: Simulation parameters for the MPTC of a FSTP inverter fed induction motor

Description	**Variables**	**Values**
Fixed-step size	-	5 μs
Solver	-	ode3
Tasking mode	-	SingleTasking
Supply voltage	V_{DC}	500 V
Damping coefficient	ξ	0.7
Natural circular pulse	ω_n	100π rad/s
Weighting factors	λ_T	0.0667 $N^{-1}m^{-1}$
	λ_φ (case 1)	1.2195 Wb^{-1}
	λ_φ (case 2)	3.6585 Wb^{-1}

Appendix E

DTC of FSTP inverter-fed induction motor

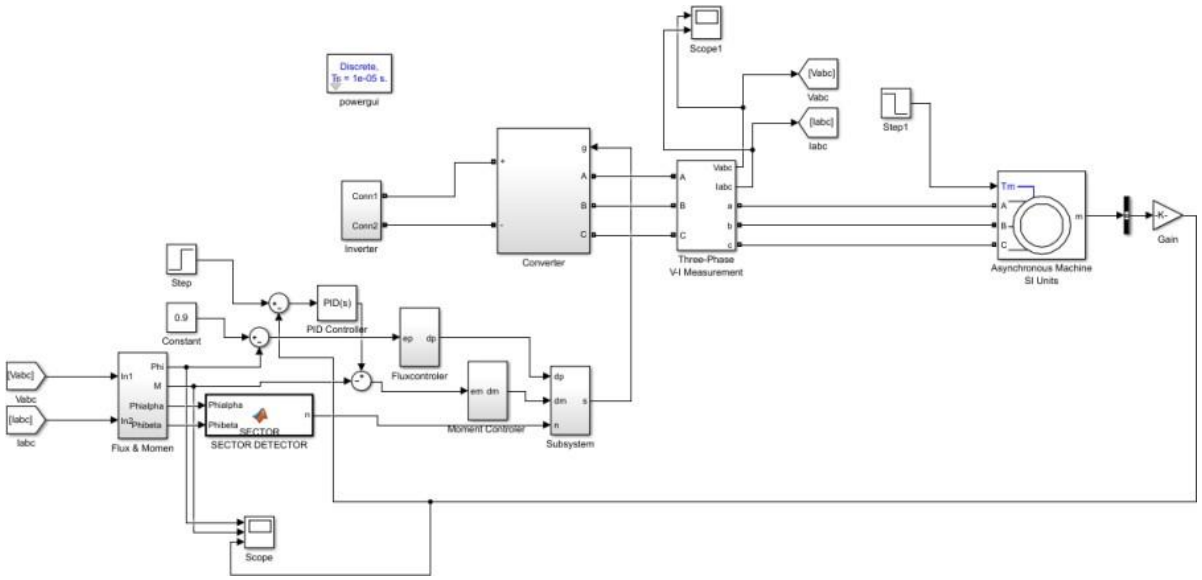

FIGURE E.1: Simulink model of the DTC of FSTP inverter-fed induction motor